Howard Hughes Medical Institute

Published as: *Cancer Cell*. 2018 February 12; 33(2): 322–336.e8.

Targeting the Senescence-Overriding Cooperative Activity of Structurally Unrelated H3K9 Demethylases in Melanoma

Yong Yu[1], **Kolja Schleich**[2], **Bin Yue**[2], **Sujuan Ji**[2,17], **Philipp Lohneis**[3,18], **Kristel Kemper**[4], **Mark R. Silvis**[5], **Nouar Qutob**[6], **Ellen van Rooijen**[7,8], **Melanie Werner-Klein**[9,10], **Lianjie Li**[2], **Dhriti Dhawan**[2], **Svenja Meierjohann**[11], **Maurice Reimann**[2], **Abdel Elkahloun**[12], **Steffi Treitschke**[13], **Bernd Dörken**[1,2,14], **Christian Speck**[15], **Frédérick A. Mallette**[16], **Leonard I. Zon**[7,8], **Sheri L. Holmen**[5], **Daniel S. Peeper**[4], **Yardena Samuels**[6], **Clemens A. Schmitt**[1,2,14,19,*], and **Soyoung Lee**[1,2,14]

[1]Max-Delbrück-Center for Molecular Medicine in the Helmholtz Association, 13125 Berlin, Germany [2]Charité - Universitätsmedizin Berlin, Corporate Member of Freie Universität Berlin, Humboldt-Universität zu Berlin, and Berlin Institute of Health, Medical Department of Hematology, Oncology and Tumor Immunology, Virchow Campus, and Molekulares Krebsforschungszentrum, 13353 Berlin, Germany [3]Charité - Universitätsmedizin Berlin, Corporate Member of Freie Universität Berlin, Humboldt-Universität zu Berlin, and Berlin Institute of Health, Institute of Pathology, 10117 Berlin, Germany [4]Division of Molecular Oncology and Immunology, The Netherlands Cancer Institute, 1066 CX Amsterdam, the Netherlands [5]Department of Surgery, University of Utah Health Sciences Center & Huntsman Cancer Institute, University of Utah, Salt Lake City, UT 84112, USA [6]Weizmann Institute of Science, Department of Molecular Cell Biology, Rehovot 7610001, Israel [7]Howard Hughes Medical Institute, Stem Cell Program and the Division of Pediatric Hematology/Oncology, Boston Children's Hospital and Dana-Farber Cancer Institute, Harvard Medical School, Boston, MA 02115, USA [8]Department of Stem Cell and Regenerative Biology, Harvard Stem Cell Institute, Cambridge, MA 02138, USA [9]Regensburg Center for Interventional Immunology (RCI) and University Medical Center of Regensburg, 93053 Regensburg, Germany [10]Experimental Medicine and Therapy Research, University of Regensburg, 93053 Regensburg, Germany [11]University of Würzburg, Physiological Chemistry, Biocenter, 97074 Würzburg, Germany [12]National Human Genome Research Institute, NIH, Bethesda, MD 20892, USA [13]Fraunhofer-Institute for Toxicology and Experimental Medicine,

[*]Correspondence: clemens.schmitt@charite.de.
[17]Present address: Chinese Academy of Medical Sciences, Peking Union Medical College, Beijing 100730, China
[18]Present address: Institute of Pathology, University Hospital Cologne, 50937 Cologne, Germany
[19]Lead Contact

SUPPLEMENTAL INFORMATION

Supplemental Information includes seven figures and two tables and can be found with this article online at https://doi.org/10.1016/j.ccell.2018.01.002.

AUTHOR CONTRIBUTIONS

Conducting Experiments, Y.Y., B.Y., S.J., P.L., K.K., M.R.S., E.v.R., L.L., D.D., S.T., M.R., and F.A.M.; Conceptual Input and Supervision, M.W.-K., C.S., B.D., S.M., L.I.Z., F.A.M., S.L.H., D.S.P., Y.S., C.A.S., and S.L.; Data Analysis, A.E., N.Q., and K.S.; Project Design and Writing, C.A.S. and S.L.

DECLARATION OF INTERESTS

L.I.Z. is a founder and stock holder of Fate Therapeutics, Marauder Therapeutics, and Scholar Rock, and a scientific advisor for Stemgent.

93053 Regensburg, Germany [14]Deutsches Konsortium für Translationale Krebsforschung (German Cancer Consortium), Partner Site Berlin, Germany [15]Institute of Clinical Sciences (ICS), Faculty of Medicine, Imperial College London, and MRC London Institute of Medical Sciences (LMS), London W12 0NN, UK [16]Department of Medicine, Université de Montré al, Maisonneuve-Rosemont Hospital Research Centre, Montré al, QC H1T 2M4, Canada

SUMMARY

Oncogene-induced senescence, e.g., in melanocytic nevi, terminates the expansion of pre-malignant cells via transcriptional silencing of proliferation-related genes due to decoration of their promoters with repressive tri-methylated histone H3 lysine 9 (H3K9) marks. We show here that structurally distinct H3K9-active demethylases—the lysine-specific demethylase-1 (LSD1) and several Jumonji C domain-containing moieties (such as JMJD2C)—disable senescence and permit Ras/Braf-evoked transformation. In mouse and zebrafish models, enforced LSD1 or JMJD2C expression promoted Braf-V600E-driven melanomagenesis. A large subset of established melanoma cell lines and primary human melanoma samples presented with a collective upregulation of related and unrelated H3K9 demethylase activities, whose targeted inhibition restored senescence, even in Braf inhibitor-resistant melanomas, evoked secondary immune effects and controlled tumor growth *in vivo*.

In Brief

Yu et al. show that two different types of histone H3 lysine 9 (H3K9) demethylases, LSD1 and JMJD2C, disable oncogenic Ras- or Braf-induced senescence by enabling the expression of E2F target genes, which permits transformation. Inhibition of the H3K9 demethylases restores senescence and controls tumor growth.

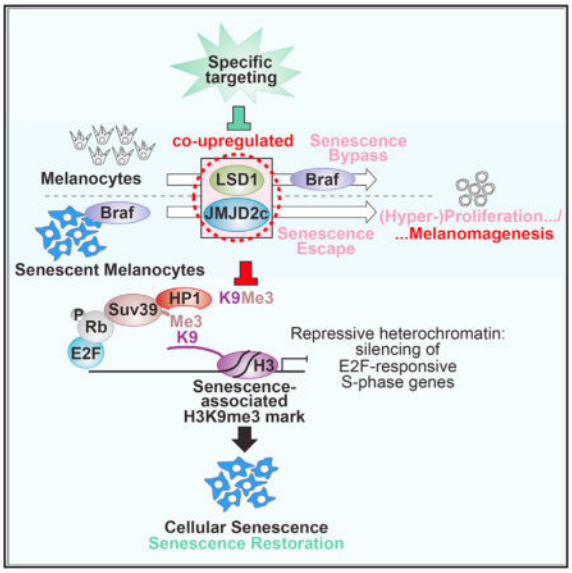

INTRODUCTION

Ras-/Raf-type oncogenes evoke a senescent cell-cycle arrest as a retinoblastoma (Rb)- and p53-dependent tumor-suppressive barrier that terminates further expansion of (pre-)malignant lesions (Collado et al., 2005; Michaloglou et al., 2005; Serrano et al., 1997). Mechanistically, Rb bound to E2F transcription factors in G_1 phase recruits histone methyltransferases that establish H3K9me3-containing chromatin marks in the vicinity of S-phase-promoting E2F target gene promoters, thereby constitutively silencing their expression (Narita et al., 2003; Zhang et al., 2005). Accordingly, we previously reported that oncogenic Ras failed to induce senescence in the absence of the Rb-associated H3K9 methyltransferase Suv39h1 in murine lymphoid cells, thus leading to Ras-driven lymphoma formation *in vivo*, which was effectively suppressed in the presence of intact *Suv39h1* alleles (Braig et al., 2005).

Histone methylation is dynamically regulated by methyltransferases and demethylases, although there is little evidence for their antagonistic operation in similar complexes at similar sets of target genes (Black et al., 2012). Specifically, structurally unrelated lysine demethylases such as the flavin-dependent amine oxidase LSD1 (AOF2 or KDM1A) and the 2-oxoglutarate (2OG)-dependent Jumonji C (JmjC) family members JMJD2C (GASC1 or KDM4C), as well as JMJD1A (KDM3A), JMJD1B (KDM3B), JMJD1C (KDM3C), JMJD2A (KDM4A), JMJD2B (KDM4B), and JMJD2D (KDM4D) reportedly possess activity against the H3K9me3 state: JMJD2C demethylates trimethylated (and also dimethylated) lysine residues of H3K9 and H3K36, while LSD1 is active on mono- or dimethylated H3K9 (H3K9me1, H3K9me2) as well as H3K4, hence eliminating the obligatory intermediates for the trimethylation step (Cloos et al., 2006; Metzger et al., 2005; Shi et al., 2004; Whetstine et al., 2006; Wissmann et al., 2007). Both enzymes were found to be overexpressed in various cancer entities, including breast, prostate, and gastrointestinal cancers, leukemia, and lymphoma (Amente et al., 2013; Berry and Janknecht, 2013). However, whether H3K9-active demethylases, whose local action is tightly controlled by expression levels and binding partners, may operate at senescence-relevant H3K9me3-decorated target genes to effectively counter oncogene-induced senescence (OIS) is not known and certainly not simply anticipatable from the opposite function an H3K9-active methyltransferase such as Suv39h1 has in OIS. Specifically, no mutual exchange of H3K9-active demethylases on one hand and Suv39h1 on the other hand in otherwise similar protein complexes has been reported so far. Moreover, given additional non-H3K9 histone and non-histone targets of LSD1 and JMJD2C, including components of the p53 pathway (Huang et al., 2007; Ishimura et al., 2009; Nicholson and Chen, 2009), it is conceivable that functions not related to H3K9 methylation might contribute to their oncogenic potential as well. If, as we hypothesize here, LSD1-and JmjC-type demethylases exert their oncogenic potential primarily at the H3K9 mark by overcoming a senescence barrier to full-blown tumor formation, this OIS relay may evolve as a potential targeting principle for senescence-restoring cancer therapies.

RESULTS

The H3K9 Demethylases LSD1 and JMJD2C Inhibit OIS

To test the impact of H3K9 demethylation on OIS, we stably introduced cDNAs encoding LSD1 and JMJD2C into wild-type mouse embryo fibroblasts (MEFs) together with oncogenic H-Ras-G12V (hereafter referred to as Ras). While Ras-expressing cells expectedly entered full-featured senescence, LSD1-or JMJD2C (as well as JMJD2A or JMJD2B)-co-expressing MEFs kept proliferating, shown by exponentially increasing cell numbers, significant colony formation, and fewer SA-β-gal-positive cells (Figures 1A–1C, S1A, and S1B). As expected, immunoblot analyses of Ras-senescent MEFs found senescence-related proteins ($p16^{INK4a}$, $p21^{CIP1}$ and H3K9me3) to be induced, whereas the expression of cyclin A and proliferating cell nuclear antigen (PCNA) encoded by E2F target genes was reduced. In contrast, Ras induction in MEFs overexpressing LSD1 or JMJD2C produced no significant changes in cyclin A and $p16^{INK4a}$, and resulted rather in slightly elevated amounts of PCNA (Figure 1D). Activation of the p53 pathway was observed following Ras expression in all three settings, implying that H3K9me3-ablating demethylase activities sufficiently block senescence irrespective of lasting $p53/p21^{CIP1}$ activation (Figure 1D). Consistent with their known specificities for mono-, di-, and trimethylated H3K9, no Ras-related changes in H3K9me1 and H3K9me2 levels became detectable in LSD1-overexpressing cells, while JMJD2C had little effect here, but, like LSD1, completely prevented an increase of H3K9me3 levels in response to Ras (Figure 1D). Notably, these findings are not restricted to murine cells. Both demethylases also canceled senescence in Ras-driven human diploid fibroblasts (HDF; Figures S1C–S1E). Overexpression of either LSD1 or JMJD2C also abrogated the Ras-dependent formation of senescence-associated heterochromatin foci and H3K9me3-positive chromatin blobs in particular (Narita et al., 2003; Zhang et al., 2005) in HDF (Figure 1E). Taken together, LSD1 and JMJD2C effectively prevent focal H3K9me3-based heterochromatinization and counter Ras-induced senescence.

LSD1 and JMJD2C Specifically Block Ras-Induced H3K9 Trimethylation of E2F Target Gene Promoters

To test whether the H3K9-active demethylases LSD1 and JMJD2C exert their senescence-compromising function at E2F target promoters, we employed chromatin immunoprecipitation (ChIP) assays. H3K9me3 occupation was observed at E2F targets (*Cdk2*, *Ccnd2*, *Ccne1*, and *Dhfr*) but not at the *Ink4a* promoter (not repressed in OIS) in Ras-senescent cells, and virtually no changes became detectable in LSD1- or JMJD2C-overex-pressing cells (Figure 2A). Consistent results were obtained at the transcript level (Figure 2B). Hence, H3K9 demethylases promote E2F target gene expression in Ras-driven cells. Moreover, additional genetic analyses ruled out that LSD1 and JMJD2C disable OIS independent of their catalytic function or via non-histone targets, specifically within the p53 pathway (Figure S2).

To further substantiate that H3K9 methylation operates as an essential component in the OIS process, we generated a histone H3 mutant with an arginine substitution of the lysine 9 residue (termed H3R9), which can no longer be methylated at this position (Tamaru and

Selker, 2001). Since it is difficult to efficiently reduce endogenous H3 expression by RNA interference due to numerous H3 genes and variants (Ederveen et al., 2011), the H3R9 cDNA was stably transferred into MEFs retaining wild-type H3, and a retrovirus encoding wild-type H3 (H3K9) was used as a control. H3R9 expression did not affect cell growth in the absence of oncogenic Ras (data not shown), but compromised senescence maintenance in Ras-driven cells after an initial growth-arrested phase (Figures 2C–2E). Consistent with nucleosome turnover required to replace some chromatin-bound wild-type H3 by a critical amount of newly synthesized H3R9, we found reduced H3K9me3 occupancy at E2F target gene promoters, but not at the *Ink4a* locus, at a late time point after H3R9 expression, while the H3K9-expressing population maintained stable H3K9me3 marks (Figure S3A). Interestingly, enforced expression of H3R9 and H3K9 was based on the his-tone variant H3.1, which, unlike H3.3, is known to require replication-coupled deposition (Ahmad and Henikoff, 2002). Since interruption of DNA replication by the S-phase blocker hydroxy-urea prevented H3R9 replacement in senescent cells (Figure S3B), we consider the possibility that histone H3 turnover in senescence is, at least in part, coupled to continuous but abortive DNA replication attempts that fail at stalled replication forks (Di Micco et al., 2006). In essence, the transcriptionally repressive H3K9me3 modification is continuously renewed during senescence and operates as an essential and demethylase-sensitive relay of OIS.

Loss of the H3K9me3 Mark Licenses Cell-Cycle Reentry Out of Cellular Senescence

If preceding expression of H3K9-active demethylases or the H3R9 mutant enables oncogenic Ras to bypass a senescence response, we hypothesized that these moieties might permit cell-cycle re-entry even after OIS has been already established. Such escape (or reversal) from OIS should be followed by proper cell divisions as the critical prerequisite for a putative oncogene-driven senescence-to-cancer transition. MEFs expressing a 4-OH-tamoxifen (4-OHT)-inducible JMJD2C-estrogen receptor (JMJD2C:ER) allele entered a robust, SA-β-gal-positive senescent arrest in response to Ras, similar to MEFs not engineered to express this fusion protein (day 9 in Figures 2F and 2G), but resumed to proliferate shortly after exposure to 4-OHT, while solvent-only-treated cells firmly remained in senescence (Figures 2F–2H). Similarly, an H3R9:ER fusion enabled Ras-senescent MEFs to divide again shortly after exposure to 4-OHT (Figures S3C–S3K). Hence, the H3K9me3 mark is not only required for efficient establishment of senescence but appears to be critical for senescence maintenance as well, with elevated activity of just a single gene product such as the H3K9 demethylase JMJD2C being sufficient to terminate the formally irreversible senescence condition.

Reduced H3K9 Trimethylation Directly Permits Malignant Transformation by Oncogenic Ras

Inactivation of cellular senescence is required for Ras-driven transformation, although the mere inability to enter senescence might not suffice to permit full-blown transformation (Peeper et al., 2001). Interestingly, overexpression of JMJD2C, but not LSD1, immortalized primary MEFs (Figure S4A). However, expression of either one, or the H3R9 mutant, directly permitted transformation in concert with Ras, to form anchorage-independent colonies, albeit with lower efficacy when compared with Ras; $Trp53^{-/-}$ cells (Figure 3A; see Figure S4B for HDF), and to grow as malignant tumors in nude mice (Figure 3B).

Furthermore, these moieties also enabled T cell lymphomagenesis in Eμ-N-Ras transgenic mice (Figure 3C), as we previously reported in this model for the absence of *Suv39h1* or *Trp53* alleles (Braig et al., 2005). In essence, H3K9-active demethylases or relative reduction of trimethylatable H3 directly permit Ras-driven tumor initiation *in vivo*.

H3K9-Active Demethylases License Braf-V600E-Driven Melanomagenesis

Nevi, potentially pre-malignant melanocytic lesions, typically develop in response to Ras or Braf activation, and represent a paradigm of OIS in humans (Michaloglou et al., 2005; Mooi and Peeper, 2006). To experimentally explore the possibilities that H3K9-active demethylases might promote bypass of or enforce escape from OIS, we stably expressed primary human melanocytes with Braf-V600E (hereafter referred to as Braf) either after (i.e., probing “senescence bypass”) or prior to (i.e., probing “senescence escape”) lentiviral transduction with JMJD2C or LSD1. Recapitulating our findings in Ras-exposed fibroblast models (Figure S5A), primary human melanocytes collectively entered senescence in response to Braf, in agreement with previous observations (Michaloglou et al., 2005), but virtually no induction of senescence became detectable in melanocytes that were engineered to overexpress LSD1 or JMJD2C prior to or after Braf activation (Figures 4A and 4B). Therefore, H3K9-active demethylases effectively counter both induction and maintenance of Ras-/Braf-evoked senescence in fibroblasts and melanocytes, with the latter capturing a key step from melanocytic nevi to malignant melanoma.

Next, we sought to directly test the impact of H3K9-active demethylases on melanomagenesis in well-established mouse and zebrafish models *in vivo*. First, an avian virus/receptor system was used to subcutaneously deliver Cre recombinase with or without LSD1 into mice harboring conditionally active Braf-V600E and floxed *Cdkn2a* alleles. While after 150 days not even half of the mice succumbed to melanoma development in the absence of LSD1 (due to the limited penetrance of the system), about 90% of the mice had already died from melanoma development prior to day 100 in the LSD1 group, typically without having deleted *Cdkn2a* (5 of the 6 tested remained $p19^{ARF}$-positive; Figure 4C). As a second model system, we probed *Tyr-Cre:ER*^{T2};*lsl-Braf*^{V600E} mice (Dankort et al., 2009; Dhomen et al., 2009), which develop senescent nevi upon Cre-mediated Braf activation via cutaneous 4-OHT exposure (Dhomen et al., 2009). LSD1- or JMJD2C-encoding lentiviruses were injected into those skin lesions, as previously shown for knockdown of PTEN that gave rise to infiltrative tumor growth at sites of injection in this model (Vredeveld et al., 2012). Strikingly, the demethylases not only licensed local melanoma formation but also promoted lymph node and distant lung metastases, as reported for homozygously *Pten*-deleted Braf-V600E-driven melanoma mice (Dankort et al., 2009) (Figures 4D and 4E). To further interrogate the role of LSD1, we used a Braf-V600E-driven, in combination with p53-deficiency, zebrafish melanoma model (Patton et al., 2005), and again found LSD1 to profoundly accelerate melanoma development (Figure 4F). Hence, H3K9-active demethylases cooperate with oncogenic Braf in the formation of aggressive melanomas by overcoming an OIS barrier *in vivo*.

Human Melanomas, but Not Senescent Melanocytic Precursors, Display High-Level Expression of H3K9-Active Demethylases

Interestingly, a transposon-mediated mutagenesis screen in Braf-mutant mice recently identified numerous candidates as contributors to melanoma progression, including the *Lsd1* and *Jmjd2c* loci (Mann et al., 2015). If H3K9 demethylases contribute to melanomagenesis, one would expect high-level expression in established melanomas, but not in senescent nevi or Braf-senescent melanocytes. First, we scanned a panel of seven human melanoma cell lines—with primary as well as Braf-senescent human melanocytes for comparison—regarding their expression levels of the H3K9me3-relevant demethylases LSD1, JMJD1A, JMJD2A, JMJD2B, and JMJD2C. While Braf induction did not significantly affect demethylase transcript levels, melanoma cell lines, in general, expressed these moieties at higher levels (Figure 5A). Independent of their Ras or Braf mutation status and origin (see Table S1), we noticed a class-wide deregulation throughout the cell lines tested: either all five demethylases were expressed at rather modestly enhanced levels (about 2- to 5-fold compared with primary melanocytes; i.e., cell lines SK-MEL-28, OMM2.3, and Mewo), or were collectively induced by more than 5-fold or even higher (i.e., cell lines A375, WM266.4, Mel202, and 92.1). Further underscored by corresponding protein levels of LSD1 and JMJD2C in the melanoma cell line panel, those with low-level demethylase expression also appeared to be the ones with the highest global H3K9me3 levels (Figure 5A). The data suggest the specific need for a critical net activity to reduce H3K9me3 levels in a subset of the melanoma cell lines. These findings further imply that other cell lines may have never experienced senescence, require lower demethylase activities to reverse OIS, or overcome this barrier primarily by a H3K9 demethylase-independent mechanism, for example by inactivating *CDKN2A* mutations as a more frequent or inactivating *TP53* mutations as a less frequent, senescence-disabling event (Serrano et al., 1997). While LSD1 accelerated melanomagenesis even in a p53-deficient background in zebrafish, the retention of *Cdkn2a* alleles, despite their flanking *loxP* sites, in LSD1-driven melanomas in the avian virus/receptor mouse model further supports this view (cf. Figure 4C, inset).

These cell-line-based findings prompted us to focus on cutaneous melanomas as a clinically highly relevant and more homogeneous entity. Hence, we next explored primary nevi or malignant melanoma tissue samples from patients. As expected, OIS-paradigmatic moles displayed profound senescence-associated H3K9me3 expression, with moderate to virtually no detectable LSD1 or JMJD2C in most samples (Figure 5B). In stark contrast, the majority of melanomas exhibited strong staining patterns for both LSD1 and JMJD2C, typically accompanied by lack of H3K9me3 reactivity (Figure 5B). Importantly, gene expression analysis of 29 human cutaneous melanomas underscored the striking association of melanoma formation with enhanced H3K9 demethylase expression, covering structurally unrelated flavin-dependent (i.e., LSD1) and 2OG-dependent (i.e., JmjC family) lysine demethylases (Figure 5C). Moreover, increased transcript levels of H3K9-active demethylases in single human disseminated melanoma cells (DMC) extended our findings to subclinical manifestations in the sentinel lymph node of clinically node-negative patients (Figure S5B). Further underscoring these results, analysis of genome-wide RNA sequencing (RNA-seq) data of melanomas from 468 patients (conducted within the Skin Cutaneous Melanoma [SKCM] project of The Cancer Genome Atlas [TCGA] Research Network)

confirmed that a large subgroup of tumors displayed high-level expression across LSD1 and JmjC family members (Figure 5D), which correlated with shorter patient survival, unleashed expression of E2F target genes, and high cell proliferation (Figures 5E, 5F, and S5C). Thus, high-level H3K9 demethylase expression is associated with bypass of or the transition from a senescent precursor to a full-blown malignancy, as it may apply to other cancer entities (see JMJD2A/lung cancer-related data in Figures S5D and S5E).

Specific Inhibition of LSD1 or JMJD2C Restores OIS

Given the prominent role of H3K9me3-active demethylases in disabling senescence and co-driving malignant transformation, we wondered whether their inhibition would suffice to restore cellular senescence as a potential anti-cancer treatment strategy. The tranylcypromine (2-phenylcyclopropylamine [2-PCPA]) para-methoxy derivative, termed 2-PCPA-1a, has been shown to effectively inhibit LSD1 including its H3K9me3-relevant demethylation activity (Pollock et al., 2012) (Figure 6A, left). Treatment of OIS-compromised Ras;LSD1 MEFs with 2-PCPA-1a restored H3K9me3-governed senescence (Figure 6A), which also could be recapitulated by genetic inhibition of LSD1 with short hairpin RNA (shRNA) (shLsd1; Figure S6A). Of note, unmodified 2-PCPA, which inhibits LSD1's effect at the H3K4 mark but has little impact on its H3K9-specific activity, failed to restore OIS, while another cyclopropylamine-based LSD1 inhibitor, GSK2879552, which is currently in clinical testing against small cell lung cancer and acute myeloid leukemia, reestablished the H3K9me3 mark as well as OIS (Figure S6B). Likewise, non-senescing Ras;JMJD2C cells exposed to IOX1, an inhibitor of JMJD2 family members (King et al., 2010), or knockdown of JMJD2C using shJmd2c paralleled the results regarding LSD1 inhibition (Figures 6B and S6C). Notably, IOX1 treatment of Ras;LSD1 and 2-PCPA-1a treatment of Ras;JMJD2C fibroblasts failed to evoke OIS, thereby underscoring their specificity for each type of demethylase, and further excluding unspecific toxicity (Figure S6D).

Next, we aimed to test the pharmacological and genetic inhibition of H3K9-active demethylases naturally selected for high expression during melanomagenesis. First, large proportions of murine B16F10 melanoma cells entered senescence when LSD1 or JMJD2C were knocked down, similar to their response to 2-PCPA-1a or IOX1 (Figure S6E). We then assessed senescence restoration in response to pharmacological inhibitors in a panel of human melanoma cell lines (cf. Figure 5A), and found the demethylase-high group to be particularly susceptible to senescence re-induction by pharmacological or genetic targeting of individual demethylases (Figures 6C, S6F–S6H, and Table S2). Of note, cell viability remained largely unaffected, and growth curve analyses mirrored the extent of senescence restoration observed in the individual cell lines (Figure S6F). As seen before in fibroblasts, LSD1 inhibition only restored senescence if a lowered E2F target-repressive H3K9me3 mark was re-established (Figure S6I). Moreover, primary human DMC also responded to LSD1 and JMJD2 inhibitors with an H3K9me3-positive restoration of senescence (Figures 6D and S6J). The senescent phenotype in three knocked down LSD1 and JMJD2C melanoma cell lines was further characterized by RNA-seq analysis (Figure 6E). Among the differentially regulated gene sets were not only E2F targets and other cell-cycle-related genes (decreased expression) but also transcripts belonging to the senescence-associated secretory phenotype (SASP) and the nuclear factor κB signaling pathway as a major driver

of pro-inflammatory SASP factors (increased expression) (Coppéet al., 2008; Kuilman et al., 2008), indicating that knockdown of LSD1 or JMJD2C indeed re-established a full-featured senescence condition in these cells.

Inhibition of H3K9 Demethylases Controls Melanoma Growth In Vivo

Finally, we aimed to exploit the efficacy and potential toxicity of demethylase inhibition *in vivo*. Indeed, repetitive intraperitoneal applications of 2-PCPA-1a or IOX1 to immunocompetent C57BL/6 mice harboring B16F10 tumors significantly attenuated melanoma expansion (Figure 7A). Importantly, mirroring induction of the SASP detected in demethylase-inactivated B16F10 cells *in vitro*, we found the senescence restoration *in situ* to be accompanied by a massive increase of melanoma-infiltrating $CD11b^+$ innate immune cells (Figure 7A), comprising granulocytes and macrophages, which reportedly clear senescent cells and may indicate an immunogenic switch of the senescence-restored melanoma cells (Xue et al., 2007). Next, we sought to monitor the *in vivo* potential of demethylase inhibition in human melanoma xenograft models and focused on three human melanoma cell lines, i.e., A375 and WM266.4, representing the demethylases-high group, and SK-MEL-28, a member of the group with less profound over-expression of H3K9me3-active demethylases. Both agents effectively controlled A375 and WM266.4, but not SK-MEL-28 tumor growth *in vivo*. Inhibitor-treated A375 and WM266.4 tumors exhibited a high fraction of SA-β-gal-positive cells *in situ*, and did not double their volume during the time the volume of solvent control-exposed tumors expanded at least 4-fold (Figure 7B).

We then probed the susceptibility of human primary melanomas to H3K9 demethylase inhibition *in vivo*. After macroscopic melanoma lesions had formed, we treated patient-derived xenograft (PDX) of Braf-V600-mutant melanomas from three individuals with similar sizes (Kemper et al., 2016) with either 2-PCPA-1a or IOX1 for more than 3 weeks. Two of the three PDX models, all showing enhanced LSD1 and JMJD2C expression levels, responded to both inhibitors with virtually overlapping and significantly slower tumor expansion compared with the DMSO-only control, while the results in the third model were promising at least regarding IOX1 (Figures 7C and S7A). Consistent with the expected pro-senescence mode of action, we found strong SA-β-gal activity and gain of a homogeneous H3K9me3 methylation pattern in tumors (Figure 7D). Thus, H3K9-demethylase-targeting therapies suppress melanoma growth *in vitro* and *in vivo* by senescence restoration, and possibly, as indicated by the syngeneic murine melanoma model, senescence-evoked host immunity. Our demethylase inhibition approach also successfully restored senescence and effectively controlled the growth of vemurafenib-resistant melanoma cell lines (Figure S7B) *in vitro* and *in vivo* (Figures 7E and 7F).

In essence, our data unmask the H3K9 chromatin mark as a melanoma vulnerability, and indicate high-level H3K9-active demethylase expression to serve as biomarker and predictor of an OIS-restoring response to LSD1 or JMJD2 inhibitors, even after failure of a Braf-targeting therapy.

DISCUSSION

Reflecting the pivotal role of OIS as a barrier to tumor formation in many pre-malignant tissues (Mooi and Peeper, 2006), senescence-disabling activities, for example inactivating alterations at the *TP53* or *CDKN2A* loci (Schmitt, 2003), are a common hallmark of cancer (Hanahan and Weinberg, 2011). We show here global H3K9 demethylase activity as a major principle to override Ras-/Braf-induced senescence, and highlight the underlying broad overexpression of structurally related and non-related H3K9 demethylase activities as a co-deregulation of shared target activities in cancer. While all H3K9 methylation "erasers" such as LSD1 and JMJD2C eventually lead to reduced levels of the OIS-essential H3K9me3 modification, further investigations are needed to unveil potential differences in H3K9me1-/2- as compared with H3K9me3-preferential demethylases regarding their role in the dynamic process of OIS induction versus maintenance. Moreover, current concepts of OIS suggest that "writers" such as Suv39h1 operate in the vicinity of critical targets via specific scaffolds, namely Suv39h1-binding Rb/E2F complexes (Nielsen et al., 2001; Rea et al., 2000), but it remains to be elucidated whether demethylases also act in a scaffold-directed manner at distinct H3K9-decorated target sites or demethylate this mark with less context specificity.

Our functional analysis provides insights into the maintenance control of the senescent cell-cycle arrest over time. Further underscoring the essential role of H3K9me3, the H3R9-based findings also characterize senescence, although viewed as a terminal arrest condition, as a much more dynamic and vulnerable state, in which methyltransferase activities are continuously needed to renew the repressive chromatin mark in the surroundings of critical target promoters, since H3-containing nucleosomes apparently undergo rapid turnover, as recently reported in the context of neuronal plasticity (Maze et al., 2015). Moreover, demethylating activities effectively counter the pro-senescent action of H3K9-targeting methyltransferases, and may even engage in common regulator networks (Piao et al., 2015). Failure to renew the H3K9me3 mark enforces cell-cycle re-entry out of senescence and hence suffices to license senescence reversal. In essence, H3K9 demethylases not only prevent senescence from being established but promote an actual senescence escape in fully arrested pre-malignant lesions as the presumably more relevant step in naturally occurring tumor development.

In turn, our data pinpoint H3K9-active LSD1 and JMJD2 family demethylases as attractive targets for future anti-cancer treatment strategies, because even relatively unselective inhibition of a contributing demethylase in tumor cells prompted rapid restoration of senescence, with globally enhanced H3K9 demethylase levels and low H3K9me3 as candidate biomarkers of response. Finally, we would also like to express a note of caution: H3K9me3-targeting in melanoma cells, which are otherwise extremely difficult to control, seems to switch them quite easily from a proliferative state into senescence—but this senescence response might not be as "irreversible" as wished for, suggesting that senescence is not an "all-or-nothing" condition but, as we speculate, can form with varying degrees of robustness. Moreover, therapeutic restoration of senescence may come with senescence-associated features such as a pro-inflammatory secretome or the acquisition of a latent stemness program (Milanovic et al., 2018), rather detrimental aspects of senescence that

warrant additional strategies to subsequently eliminate these senescence-restored cancer cells for improved long-term outcome (Dorr et al., 2013).

Given the enhanced immune cell invasion and tumor-immune interaction observed here and in various settings after senescence induction *in vivo* (Kang et al., 2011; Xue et al., 2007), the ability of vemurafenib to induce senescence in Braf-mutant melanomas (Haferkamp et al., 2013), and our approach presented here to inhibit H3K9-active demethylases irrespective of acquired insensitivity to vemurafenib, we would like to envision a chemo-free triple-targeting strategy for melanoma (and possibly other cancer entities) that integrates effective suppression of Braf/MEK oncogenic signaling (Robert et al., 2015), immune therapy via checkpoint blockade (Postow et al., 2015), and, in a presumably synergistic fashion, senescence restoration via demethylase inhibition.

STAR★METHODS

KEY RESOURCES TABLE

REAGENT or RESOURCE	SOURCE	IDENTIFIER
Antibodies		
H3K9me3	Abcam	Cat#ab8898; RRID: AB_306848
H3K9me2	Cell Signaling Technology	Cat#4658S; RRID: AB_10544405
H3K9me	Abcam	Cat#ab8896; RRID: AB_732929
H3	Cell Signaling Technology	Cat#4499S; RRID: AB_10544537
H3K27me3	Cell Signaling Technology	Cat#9733S; RRID: AB_2616029
H3K4me3	Cell Signaling Technology	Cat#9751S; RRID: AB_2616028
H2A	Cell Signaling Technology	Cat#12349S; RRID: AB_2687875
Ras	Santa Cruz Biotechnology	Cat#sc-68743; RRID: AB_2264392
JMJD2C	Abcam	Cat#ab85454; RRID: AB_2129195
JMJD2A	Cell Signaling Technology	Cat#5328S; RRID: AB_10828595
LSD1	Cell Signaling Technology	Cat#2184S; RRID: AB_2070132
$p21^{CIP1}$	Santa Cruz Biotechnology	Cat#sc-397; RRID: AB_632126
$p16^{INK4a}$	Santa Cruz Biotechnology	Cat#sc-1661; RRID: AB_628067
Phospho-Rb (Ser780)	Cell Signaling Technology	Cat#8180S; RRID: AB_10950972
p53	Leica Biosystems	Cat#NCL-p53-CM5p; RRID: AB_563933
p53 phospho-S15	Cell Signaling Technology	Cat#9284S; RRID: AB_331464
Cyclin A	Sigma	Cat#C4710; RRID: AB_1078603
PCNA	Cell Signaling Technology	Cat#2586S; RRID: AB_2160343
FLAG	Sigma	Cat#F3165; RRID: AB_259529
Ki67	Thermo Scientific	Cat#MA5-14520; RRID: AB_10979488
CD3	Novocastra	Cat#MAB9626; RRID: AB_10774049
B220	BD Biosciences	Cat#550286; RRID: AB_393581
Braf-V600E	Ventana Medical Systems	Cat#790-4855
α-Tubulin	Sigma	Cat#T5168; RRID: AB_477579
horseradish peroxidase-conjugated goat- anti-rabbit	GE Healthcare	Cat#RPN4301; RRID: AB_2650489
horseradish peroxidase-conjugated sheep- anti-mouse	GE Healthcare	Cat#NA931V; RRID: AB_772210
Bacterial and Virus Strains		
pCDH-CMV-MCS-EF1-GFP	System Biosciences	CD511B-1
MSCV Retroviral Expression System	Clontech	634401
replication-competent avian leucosis virus (RCAS)	VanBrocklin et al., 2010; Cho et al., 2015	N/A
Biological Samples		

REAGENT or RESOURCE	SOURCE	IDENTIFIER
Human nevi and melanomas	Charité–University Medical Center, Berlin	N/A
Disseminated melanoma cells	University Regensburg	14-01-47, 102-4
Patient-derived xenografts (PDX)	The Netherland Cancer Institute	M026.X2, M029.X2, M032.X2
Chemicals, Peptides, and Recombinant Proteins		
LSD1 inhibitor: 2-PCPA-1a	Uorsy, Ukraine	BBV27286962
JMJD2C inhibitor: IOX1	Sigma	SML0067
LSD1 inhibitor: 2-PCPA	Cayman Chemical	10010494
LSD1 inhibitor: GSK2879552	Active Biochem	A-1385
Braf-V600 inhibitor: Vemurafenib	Selleckchem	S1267
4-hydroxy tamoxifen (4-OHT)	Sigma	H6278
Hydroxyurea	Sigma	H8627
Critical Commercial Assays		
iDeal ChIP-seq kit for Histones	Diagenode	C01010051
REAL™ Detection System, Alkaline Phosphatase_RED, Rabbit_Mouse	Dako	K5005
GeneCatcher™ gDNA Blood Kit	Invitrogen	CS21110
Nuclear Extraction Kit	Abcam	ab113474
Deposited Data		
Raw and analyzed data on RNA-seq based gene expression quantification in human melanoma cell lines after shRNA-mediated knockdown of JMJD2C or LSD1	This paper	GSE105137; https://www.ncbi.nlm.nih.gov/geo/query/acc.cgi?acc=GSE105137
Raw and analyzed data on RNA-seq based gene expression quantification in one mouse melanoma cell line after shRNA-mediated knockdown of JMJD2C or LSD1	This paper	GSE105138; https://www.ncbi.nlm.nih.gov/geo/query/acc.cgi?acc=GSE105138
Human reference genome NCBI build 38, GRCh38 Ensembl release 88	Genome Reference Consortium	ftp://ftp.ensembl.org/pub/release-88/fasta/homo_sapiens/dna/Homo_sapiens.GRCh38.dna.primary_assembly.fa.gz
Mouse reference genome NCBI build 38, GRCm38 Ensembl release 88	Genome Reference Consortium	ftp://ftp.ensembl.org/pub/release-88/fasta/mus_musculus/dna/Mus_musculus.GRCm38.dna.primary_assembly.fa.gz
Experimental Models: Cell Lines		
Mouse: melanoma cell line B16F10	Laboratory of Gerald Willimsky	RRID: CVCL_0159
Human: melanoma cell lines 92.1 (female)	Laboratory of Martine J. Jager	RRID: CVCL_8607
Human: melanoma cell lines Mel202 (female)	Laboratory of Martine J. Jager	RRID: CVCL_C301
Human: melanoma cell lines OMM2.3 (male)	Laboratory of Martine J. Jager	RRID: CVCL_C306
Human: melanoma cell lines A375 (54-year-old female)	ATCC	Cat#CRL-1619; RRID: CVCL_0132
Human: melanoma cell lines SK-MEL-28 (51-year-old male)	ATCC	Cat#HTB-72; RRID: CVCL_0526;
Human: melanoma cell lines Mewo (78-year-old male)	ATCC	Cat#HTB-65; RRID: CVCL_0445
Human: melanoma cell line WM266.4 (55-year-old female)	Biomol	Cat#WM266-4-01; RRID: CVCL_2765
Human: primary melanocytes	Thermofisher Scientific	Cat#C0025C
Human: diploid fibroblast	Laboratory of Daniel Peeper	Tig3; RRID: CVCL_E939
Mouse: primary embryonic fibroblasts	Own production	MEF
Experimental Models: Organisms/Strains		
Mouse: *Crl:NU-Foxn1-nu/nu*	Charles River, Germany	490
Mouse: C57BL/6	Charles River, Germany	027
Mouse: *Trp53*$^{-/-}$	Jacks et al., 1994	N/A
Mouse: *Suv39h1-*	Peters et al., 2001	N/A
Mouse: Eμ-N-Ras	Haupt et al., 1992	N/A
Mouse: *K-Ras*^{LA2}	Johnson et al., 2001	N/A
Mouse: *Tyr::CreER;Braf*$^{CA/+}$	Svenja Meierjohann (Dankort et al., 2009)	N/A
Mouse: *Dct::TVA;Braf*$^{CA;Cdkn2a\ lox/lox}$	VanBrocklin et al., 2010	N/A
Mouse for human melanoma PDX transplantation: NOD.*Cg-Prkdc*^{scid}*Il2rg*^{tm1Wjl}/*SzJ* (NSG)	The Netherland Cancer Institute	NSG

REAGENT or RESOURCE	SOURCE	IDENTIFIER
Zebrafish: Tg(*mitfa:BRAF*^{V600E});*p53*$^{-/-}$;*mitfa*$^{-/-}$	Ceol et al., 2011	N/A
Oligonucleotides		
shRNA targeting sequence: human *LSD1*: AGGAAGGCTCTTCTAGCAATA	This paper	sh*LSD1*
shRNA targeting sequence: human *JMJD2C*: GCAGAGAGTAATGGTGTGTTA	This paper	sh*JMJD2C*
shRNA targeting sequence: murine *Lsd1*: GCTGAAGGCTTGGACATTAAA	This paper	sh*Lsd1*
shRNA targeting sequence: murine *Jmjd2c*: GCAGAGTGATAGATGTGACAT	This paper	sh*Jmjd2c*
shRNA targeting sequence: murine *Mdm2*: GTGACGACTATTCCCAACCAT	This paper	sh*Mdm2*
ChIP primer sequence for human *DHFR*: CAAGCCCCCTCATCAGAAT	This paper	hDHFR-Fwd
ChIP primer sequence for human *DHFR*: GGTGAAGCGCTGAGGTTTT	This paper	hDHFR-Rev
ChIP primer sequence for human *INK4A*: GTCCTCCTTCCTTGCCAAC	This paper	hINK4A-Fwd
ChIP primer sequence for human *INK4A*: AATGTGGCACCCCTGAAGT	This paper	hINK4A-Rev
ChIP primer sequence for murine *Dhfr*: GCGGAGCCGTACTTTACCT	This paper	mDhfr-Fwd
ChIP primer sequence for murine *Dhfr*: GGGAGGCAAACGGTTCTAA	This paper	mDhfr-Rev
ChIP primer sequence for murine *Cdk2*: CCGACACTCGGAGCGGAGGA	This paper	mCdk2-Fwd
ChIP primer sequence for murine Cdk2: CCGCCCTCGTGACGTGAACC	This paper	mCdk2-Rev
ChIP primer sequence for murine *Ccnd2*: GGGCCAATGGAACCACGCCT	This paper	mCcnd2-Fwd
ChIP primer sequence for murine *Ccnd2*: CCAGCGGTTGGGCAGCCA	This paper	mCcnd2-Rev
ChIP primer sequence for murine *Ccne1*: ATAGCGAGCCAGCAGGGACC	This paper	mCcne1-Fwd
ChIP primer sequence for murine *Ccne1*: AGGAGCCCAGGAGAGTGGGGT	This paper	mCcne1-Rev
ChIP primer sequence for murine *Ink4a*: CGCAAAGATTCGGATTTCA	This paper	mInk4a-Fwd
ChIP primer sequence for murine *Ink4a*: CAACTTCGCCAAGCTGAGA	This paper	mInk4a-Rev
Recombinant DNA		
cDNA: murine LSD1	Dharmacon	MMM1013-202798746
cDNA: murine JMJD2C	Dharmacon	MMM1013-202766942
cDNA: human LSD1	Dharmacon	MHS6278-202806727
cDNA: human JMJD2C	Dharmacon	MHS6278-202857855
cDNA: mouse JMJD2A	Dharmacon	MMM1013-202765244
cDNA: mouse JMJD2B	Dharmacon	MMM1013-202761698
Mutant mouse LSD1	This paper	LSD1-K661A
Mutant mouse JMJD2C	This paper	JMJD2C-H190A
Histone H3.1 H3K9	This paper	H3K9
Histone H3.1 H3R9 mutant	This paper	H3R9
Ras-G12V	This paper	N/A
Braf-V600E	This paper	N/A
Plasmid: PMX-pie-JMJD2C:ER-puro-GFP	This paper	JMJD2C:ER
Plasmid: PMX-pie-H3R9:ER-puro-GFP	This paper	H3R9:ER
Plasmid: PMX-pie-Ras:ER-puro-GFP	This paper	Ras:ER
Plasmid: Gateway pENTR™ 1A Dual Selection Vector	Thermofisher scientific	A10462
Plasmid: G_1 cell cycle marker pRetroX-G1-Red Vector	Clontech	631463
Plasmid: pSuper-retro-puro	Oligoengine	VEC-pRT-0002
Plasmid: pBabe-3×FLAG-puro	This paper	N/A
Plasmid: PMX-pie-3×FLAG-ER-puro-GFP	This paper	N/A

REAGENT or RESOURCE	SOURCE	IDENTIFIER
Software and Algorithms		
Prism 5	Graphad	RRID: SCR_015807
FlowJo 8.8.6	FlowJo	RRID: SCR_008520
SortMeRNA version 2.1	Kopylova et al., 2012	http://bioinfo.lifl.fr/RNA/sortmerna/
STAR RNA-seq aligner version 2.5.2b	Dobin et al., 2013	https://github.com/alexdobin/STAR
Samtools version 0.18		http://www.htslib.org/
Samtools version 1.4		http://www.htslib.org/
FastQC version 0.11.5	Babraham Bioinformatics	https://www.bioinformatics.babraham.ac.uk/projects/fastqc/
R/Bioconductor		https://www.bioconductor.org/
Other		
Skin Cutaneous Melanoma Gene Expression	GDC Data Portal: TCGA-SKCM	https://portal.gdc.cancer.gov/
Skin Cutaneous Melanoma Simple Nucleotide Variation, Data Category: Masked Somatic Mutation, Workflow Type: MuSe Variant Aggregation and Masking	GDC Data Portal: TCGA-SKCM	TCGA.SKCM.muse.bc35087a-858d-4859-8183-ddf3e342acac.DR-6.0.somatic.maf.gz
HomoloGene release 68	NCBI HomoloGene	ftp://ftp.ncbi.nih.gov/pub/HomoloGene/build68/homologene.data
Molecular Signature Database v6.0		http://software.broadinstitute.org/gsea/msigdb
KEGG: Kyoto Encyclopedia of Genes and Genomes		http://www.genome.jp/kegg/kegg2.html
Cell cycle signature	KEGG	04110
NF-κB signature	KEGG	04064
HALLMARK_E2F_TARGETS signature	MSigDB	
SASP signature	Coppe et al., 2010	Table 1
	Pribluda et al., 2013	Figure 2D SASP genes
	Kuilman & Peeper, 2009	Table 1

CONTACT FOR REAGENT AND RESOURCE SHARING

Further information and requests for resources and reagents should be directed to and will be fulfilled by the Lead Contact, Clemens A. Schmitt (clemens.schmitt@charite.de).

EXPERIMENTAL MODEL AND SUBJECT DETAILS

All animal protocols used in this study were approved by the local governmental review board according to the location where each experiment was carried out (animal experimental committee of the NKI, Amsterdam, the Netherlands; Landesamt Berlin, Germany; Boston Children's Hospital (BCH) Institutional Animal Care and Use Committee (IACUC), Boston, USA; University of Utah Institutional Animal Care and Use Committee (IACUC), Salt Lake City, USA; Animal Care Committee at McGill University, Montréal, Canada) and conform to the regulatory standards. Gender of animals used in different *in vivo*-models are mentioned in each section. Primary MEFs were isolated from E13.5 embryos, and their gender is not available. Gender identity of cell lines is listed in the Key Resources Table.

Braf Mice—The activation of $Braf^{V600E}$ by topical administration of 4-OHT onto the skin of $Tyr::CreER;Braf^{CA/+}$ mice has been described in (Dankort et al., 2009). The gender of the mice was mixed and no influence on penetrance or latency was observed. After the observation of Braf-induced pigmented regions, mice received total body γ-irradiation at a sublethal dose (5 Gy) (Vredeveld et al., 2012), 3 days prior to the subcutaneous injection of lentivirus co-encoding murine LSD1, JMJD2C, or empty vector with GFP. The lentivirus was produced in 293T cells using the pCDH-CMV-MCS-GFP vector as backbone.

TVA RCAS Melanoma Model—The dopachrome tautomerase promoter-driven tumor virus A receptor-expressing mice (Dct::TVA) mice engineered to harbor a conditionally active Braf-V600E and floxed *Cdkn2a* alleles (*Dct::TVA;Braf*^{CA};*Cdkn2a*$^{lox/lox}$) were generated as previously described (VanBrocklin et al., 2010). All animal experimentation was performed in Association for Assessment and Accreditation of Laboratory Animal Care (AAALAC)-approved facilities at the University of Utah. All animal protocols were reviewed and approved prior to experimentation by the Institutional Animal Care and Use Committee at the University of Utah. The gender of the mice was mixed and no influence on penetrance or latency was observed. Retroviral vectors utilized for this model are replication-competent avian leukosis virus, Bryan polymerase-containing vectors of envelope subgroup A (designated RCASBP[A] and abbreviated RCAS) (VanBrocklin et al., 2010). RCAS-3x-FLAG *LSD1* was created by mixing pENTR1A-3x-FLAG *LSD1* with the RCAS destination vector in the presence of the Gateway LR Clonase II Enzyme Mix (Invitrogen) and verified by sequencing. Generation and propagation of RCAS virus and *in vivo*-infection of *Dct::TVA;Braf*^{CA};*Cdkn2a*$^{lox/lox}$ mice were previously described (Cho et al., 2015).

Melanoma PDX—Generation of the PDX was performed as described previously (Kemper et al., 2016). All patients have signed informed consent for the study (N03LAM), which was approved by the Medical Ethical Review Board of the Antoni van Leeuwenhoek, the Netherlands. Passage 2-PDX was enzymatically dissociated, and 250.000 cells were injected per flank of 6–7 week old NOD.*Cg-Prkdc*^{scid}*Il2rg*^{tm1Wjl}/SzJ (NSG) mice (in-house bred). When tumors reached the volume of about 50 mm^3, treatment was initiated by intraperitoneally administering inhibitors every two days, *i.e.* either 2-PCPA-1a (12.5 mg/kg), IOX1 (2.5 mg/kg), both dissolved in DMSO/PBS, or solvent-only as a control.

Zebrafish Melanoma Model and MiniCoopR System—Zebrafish develop melanoma when melanocytes express human oncogenic Braf-V600E in a *tp53*-deficient background (Patton et al., 2005). When crossed to a *mitfa* loss-of-function mutant, melanocyte development is impaired and melanoma no longer form. Injection of the transposon-based expression vector MiniCoopR (MCR) into Tg(*mitfa:BRAF*^{V600E});*tp53*$^{-/-}$;*mitfa*$^{-/-}$ one-cell stage zebrafish embryos rescues melanocytes by restoring *mitfa*, and simultaneously allows the expression of a candidate gene in the rescued pigment lineages (Ceol et al., 2011). MCR expression constructs were created by MultiSite Gateway recombination (Invitrogen) using full-length human open reading frames. Briefly, 25 pg of MCR:LSD1 or MCR:EGFP were microinjected together with 25 pg of Tol2 transposase mRNA into one-cell Tg(*mitfa:BRAF*^{V600E});*tp53*$^{-/-}$;*mitfa*$^{-/-}$ zebrafish embryos. Embryos were scored for melanocyte rescue at 48–72 hours post-fertilization, and equal numbers were raised to adulthood, and scored weekly (8–12 weeks) or biweekly (> 12 weeks) for the emergence of melanoma lesions. Zebrafish were maintained under Institutional Animal Care and Use Committee-(IACUC)-approved conditions.

K-Ras Lung Cancer Model—To detect JMJD2A in the lung of the K-Ras lung cancer mouse model (Johnson et al., 2001), paraffin-embedded samples were stained with a JMJD2A antibody (Cell Signaling, 1:20). Retroviral plasmids encoding JMJD2A (pLPC-

flag-JMJD2A) or a small-hairpin against p53 (shp53), and infections of IMR90 cells were previously described (Mallette and Richard, 2012).

METHOD DETAILS

Plasmids and Retroviral Gene Transfer—Full-length cDNAs of *Lsd1* and *Jmjd2c* were purchased from GE Healthcare Dharmacon. $HRAS^{G12V}$, $ER{:}HRAS^{G12V}$, *Jmjd2c*, $Jmjd2c^{H190A}$, *Lsd1*, $Lsd1^{K661A}$, histone H3K9 and histone H3R9 (both H3K9 and H3R9 were constructed from the H3.1 isoform, with the arginine 9 derivative generated by an A-to-G exchange at nucleotide position 29) were subcloned into murine stem cell retrovirus (MSCV) backbones co-encoding blasticidine or puromycin antibiotic resistance genes. Inducible JMJD2C:ER and H3R9:ER constructs were made by using the pMX-pie plasmid (Littlewood et al., 1995). shRNA sequences to knock-down LSD1, JMJD2C, and MDM2 are listed in the Key Resources Table. Retroviral gene transfer and antibiotic selection of MEFs or HDFs were previously described (Schmitt et al., 2002).

To induce the activity of ER-fusion proteins, cells were incubated with 100 nM 4-hydroxy-tamoxifen (4-OHT, Sigma), freshly provided every two days when the medium was regularly exchanged. To restore OIS *in vitro*, 200 μM of 2-PCPA-1a or 10 μM of IOX1 (dissolved in DMSO), or a solvent control, were applied for 4 days, unless indicated otherwise.

Cell Proliferation Assays and SA-β-Gal Staining—Cell-cycle distribution was measured *via* incorporation of BrdU (Molecular Probes) and PI labeling by flow cytometry as described (Reimann et al., 2010). For growth curve analyses, 2×10^4 MEFs were seeded in 12-well plates, or 1×10^5 Tig3 cells were plated in 6-well plates and counted at the indicated time-points, and eventually stained with crystal violet at day 9. SA-β-gal staining was carried out *in vitro* and *in vivo* as previously described (Braig et al., 2005; Dimri et al., 1995; Jing et al., 2011).

3T1 Protocol—To immortalize primary MEFs, a modified 3T3 protocol (Todaro and Green, 1963) was employed. Briefly, low-passage MEFs were retrovirally infected as indicated and propagated on a defined 3-day passage schedule by plating 1×10^5 cells (*i.e.* “3T1”) per well in 6-well plates. Cells were counted at each passage to determine the number of divisions.

Anchorage-Independent Colony Formation—Colony formation in semi-solid medium was measured in 12-well plates. 3.000 cells in a 0.3% agarose/DMEM/FBS single-cell suspension were plated as upper layer onto a bottom layer of 0.5% low-melting agarose (Invitrogen) in DMEM supplemented with 10% FBS. Fresh medium was added on top of the agar every three days, and the plates were stained with 0.05% crystal violet to visualize colonies after two weeks.

Immunoblotting, Immunohistochemistry and Immunofluorescence—Immunoblotting (IB), immunohistochemistry (IHC) and immunofluorescence staining (IF) were carried out as previously described (Jing et al., 2011; Schmitt et al., 1999). For detailed information of antibodies, please see Key Resources Table. For nevi and melanoma IHC

(Figure 5B), anonymous patients permitted use of leftover tissue for scientific purposes, as stipulated in the standard treatment contract signed by the patients of the Charité - University Medical Center, Berlin, Germany. Staining intensity was classified (weak, moderate, strong) by unbiased examiners.

Chromatin Immunoprecipitation (ChIP) Assays and Quantitative RT-PCR (qRT-PCR) Analyses—ChIP assays were performed using the ChIP-IT Express Chromatin Immunoprecipitation Kit (Active Motif) with primer pairs specific for the promoters of *Cdk2*, *Ccnd2*, *Ccne1*, *Dhfr* and *Ink4a* genes. Primer sequences are available upon request. For qRT-PCR, RNA was extracted with TRIzol (Invitrogen) and transcribed into cDNA using SuperScriptIII reverse transcriptase (Invitrogen) primed by oligo-dT according to manufacturer's instructions. Transcript expression levels of murine *Cdk2*, *Ccnd2*, *Ccne1*, *Dhfr*, *Ink4a*, and human *LSD1*, *JMJD1A*, *JMJD2B*, *JMJD2*C were measured using commercially available primers (Applied Biosystems) and calculated relative to the expression of GAPDH as a housekeeping control mRNA (Jing et al., 2011).

Tumorigenicity of Genetically Engineered MEFs and FLCs—Tumorigenicity was tested by subcutaneously injecting 2×10^6 MEFs (harboring the indicated defined genetic lesions) on each flank of 5–6 weeks old *Crl:NU-Foxn1-nu/nu* mice (Charles River, Germany). Inoculation sites were inspected regarding tumor growth three times a week, and tumors were measured using a caliper ruler in two perpendicular dimensions to calculate the tumor volume by the modified ellipsoidal formula (tumor volume = $0.5 \times \text{length} \times \text{width}^2$; with the length being the longest diameter and the width a perpendicular diameter (Euhus et al., 1986)). Isolation, retroviral infection, and transplantation of Eμ-N-Ras transgenic fetal liver cells infected with LSD1 or JMJD2C constructs were performed as previously described (Schmitt et al., 2002).

Inhibitor Treatment—For *in vivo*-treatments, 1×10^6 cells were implanted subcutaneously into the flanks of 5–6 weeks old *Crl:NU-Foxn1-nu/nu* mice (Charles River, Germany) regarding human melanoma cell lines, or into syngeneic wild-type C57BL/6 mice when implanting murine B16F10 melanoma cells, and resulting tumors were monitored as described above for MEF transplantation. When tumors reached a volume of about 200 mm^3, treatment was started by intraperitoneally administering inhibitors three times a week, *i.e.* either 2-PCPA-1a (12.5 mg/kg), IOX1 (2.5 mg/kg), or DMSO as a solvent control.

Live Cell Imaging—MEFs stably expressing the G_1-phase cell-cycle marker pRetroX-G1-Red (Clontech), Ras, and either JMJD2C:ER or H3R9:ER were seeded in ibidi μ-slide 8-well chamber (cat. no. 80827). Monitoring and live cell imaging started right after the addition of 4-OHT or EtOH as vehicle control using the BD Pathway 855 Bioimager system. Images were captured every hour over 5 days and processed with the Bioimager AttoVision and Adobe Photoshop software packages.

Culture and Infection of Primary Human Melanocytes—Human primary melanocytes were obtained from Life Technologies and cultured under the condition recommended by the supplier. Cells were infected with lentiviruses encoding Braf-V600E,

human LSD1, JMJD2C, or an empty vector. Senescence was visualized by SA-β-gal staining 5 days after infection, and crystal violet staining was performed after 3 weeks.

Culture and Growth Analysis of Patient-Derived Disseminated Melanoma Cells (DMCs)—The study using DMC was approved by the ethics committee of the University Regensburg, Germany (07-079). Single DMCs were isolated from sentinel lymph nodes of melanoma patients without distant metastasis (M0). DMCs used in this study harbor either a Braf exon 15 mutation (c1799T>A) or an N-Ras exon 3 mutation (c181C>A), as determined by Sanger sequencing (Sequiserve, Vaterstetten, Germany). Their patient-origin was verified by short tandem repeat (STR) analysis (Cell-ID™, Promega), their melanoma-origin was confirmed by the pathologist and their aberrant genotype by comparative genomic hybridization. DMCs were maintained in RPMI 1640 medium containing 10% FBS, 1× Glutamax (Life Technologies) and 50 units/ml penicillin/streptomycin, and routinely tested for the absence of mycoplasma. To measure cell proliferation, cells were first labeled with 4 μM CellTrace Violet (Life Technologies) in PBS/1% FBS for 20 min, washed with PBS/10% FBS, and then treated with 200 μM 2-PCPA-1a or 10 μM IOX1. After four to eleven days (depending on the doubling time of individual DMCs), cells were trypsinized, stained with the viability dye eFlour 780 (ebioscience), and the dilution of Celltracer violet was assessed by flow cytometry. Data were analyzed with the FlowJo 8.8.6 software package.

Generation of Vemurafenib-Resistant Melanoma Cell Lines—To generate Vemurafenib-resistant cells, human melanoma cell lines A375 and WM266.4 were cultured with increasing concentrations of the Braf-V600E inhibitor Vemurafenib (0.2–1 μM) for 30 days, with the medium being regularly exchanged.

QUANTIFICATION AND STATISTICAL ANALYSIS

Statistical Analyses—Statistical differences between two experimental groups were calculated using the unpaired two-tailed Student's *t*-test. Statistical differences of growth curves (cell numbers and tumor volumes) were calculated using the two-way ANOVA test if not otherwise indicated. A significance level of $p < 0.05$ was used throughout the study. Kaplan-Meier curves representing survival analyses were compared by the log-rank (Mantel-Cox) test using the Prism software package (GraphPad) or the *survival* package in R.

Gene Expression and Hierarchical Clustering Analyses of Melanoma Patient Samples—Gene expression profiles for 29 melanoma patient samples (Gartner et al., 2013) were measured using Affymetrix human exon 1.0 ST version 2: HuEx-1_0-st-v2 arrays. The scanned array images were processed and analyzed using Partek Genomics Suite software, version 6.6 Copyright 2014 Partek Inc., St. Louis, MO, USA. Gene expression data of control melanocytes were generated from the GSE15281 GEO dataset. Clustering was performed in R and the resulting dendrograms were re-ordered based on median gene expression.

Bioinformatics—Gene expression data analysis was conducted in R/Bioconductor using custom scripts and various packages including *clusterProfiler* for Gene Set Enrichment Analysis and *DESeq2* for Differential Expression Analysis.

Gene Signatures—The Cell cycle (04110) and NF-κB (04064) signatures were taken from KEGG and the E2F targets signature was taken from the Molecular Signatures Database (MSigDB). The SASP signature was compiled from literature sources (Coppe et al., 2010; Kuilman and Peeper, 2009; Pribluda et al., 2013). Additional details are shown in the Key Resources Table.

RNA-Seq Pre-processing—The BGI pre-filtered sequencing reads were subjected to computational rRNA depletion using SortMeRNA (Kopylova et al., 2012), against all eight provided databases, followed by mapping to human or mouse reference genomes using STAR aligner (Dobin et al., 2013) in per-sample 2-pass mode. As reference genomes we used GRCh38.88 for human and GRCm38.88 for mouse, respectively. Transcript abundance was subsequently quantified using the summarizeOverlaps function from the R/Bioconductor *GenomicAlignments* package in "Union" mode. Raw transcript counts were transformed to log2 scale using *rlog* from the *DESeq2* package, which also normalizes for sequencing depth.

TCGA Data Analysis—RNA-seq based gene expression data from the TCGA-SKCM project was downloaded from the GDC data portal using the R/Bioconductor package *TCGAbiolinks*. This expression dataset comprised 470 metastatic and primary solid skin cutaneous melanoma samples from 468 patients. Raw transcript counts were transformed to log2 scale after normalizing for sequencing depth and adding a pseudo-count of one. For survival analysis, still living patients were included as censored data using time to last follow-up. The SNV dataset included samples from 467 patients.

Conversion of Gene Signatures between Organisms—Gene signatures were converted between human and mouse, using data from NCBI HomoloGene relase 68. In addition, corresponding gene symbols, not listed in HomoloGene, were converted by searching for the capitalized lowercase (human-to-mouse) or the uppercase version (mouse-to-human) symbol in organism-specific R/Bioconductor annotation packages.

DATA AND SOFTWARE AVAILABILITY

The accession number for RNA sequencing data reported in this study is GEO: GSE105137 and GSE105138.

Supplementary Material

Refer to Web version on PubMed Central for supplementary material.

Acknowledgments

We thank T. Jacks, T. Jenuwein, P. Khavari, S. Lowe, Ó. Fernándes-Capetillo, G. Willimsky, and M.J. Jager for reagents and mice, E. Berg, K. Reimers, N. Burbach, A. Herrmann, and S. Maβwig as well as the Intervention Unit at the Netherlands Cancer Institute for technical assistance, and members of the Schmitt lab for discussions and

editorial advice. This work was supported by grants from the Deutsche Forschungsgemeinschaft (TRR 54) and the German Cancer Consortium (Deutsches Konsortium für Translationale Krebsforschung [DKTK]) to C.A.S. and S.L.; Wilhelm Sander Foundation (2015.016.1) to M.W.-K.; NIH funding (R01 no. CA103846), a market readiness assistance grant, and the Ellison Foundation to L.I.Z.; Chinese Scholarship Council stipends to Y.Y., B.Y., and L.L.; a Berlin School of Integrative Oncology (BSIO) stipend to D.D.; ERC (StG-335377) to Y.S.; and the Canadian Institutes of Health Research (MOP-133442) to F.A.M.

References

Ahmad K, Henikoff S. The histone variant H3.3 marks active chromatin by replication-independent nucleosome assembly. Mol Cell. 2002; 9:1191–1200. [PubMed: 12086617]

Amente S, Lania L, Majello B. The histone LSD1 demethylase in stemness and cancer transcription programs. Biochim Biophys Acta. 2013; 1829:981–986. [PubMed: 23684752]

Berry WL, Janknecht R. KDM4/JMJD2 histone demethylases: epigenetic regulators in cancer cells. Cancer Res. 2013; 73:2936–2942. [PubMed: 23644528]

Black JC, Van Rechem C, Whetstine JR. Histone lysine methylation dynamics: establishment, regulation, and biological impact. Mol Cell. 2012; 48:491–507. [PubMed: 23200123]

Braig M, Lee S, Loddenkemper C, Rudolph C, Peters AH, Schlegelberger B, Stein H, Dorken B, Jenuwein T, Schmitt CA. Oncogene-induced senescence as an initial barrier in lymphoma development. Nature. 2005; 436:660–665. [PubMed: 16079837]

Ceol CJ, Houvras Y, Jane-Valbuena J, Bilodeau S, Orlando DA, Battisti V, Fritsch L, Lin WM, Hollmann TJ, Ferre F, et al. The histone methyltransferase SETDB1 is recurrently amplified in melanoma and accelerates its onset. Nature. 2011; 471:513–517. [PubMed: 21430779]

Cho JH, Robinson JP, Arave RA, Burnett WJ, Kircher DA, Chen G, Davies MA, Grossmann AH, VanBrocklin MW, McMahon M, et al. AKT1 activation promotes development of melanoma metastases. Cell Rep. 2015; 13:898–905. [PubMed: 26565903]

Cloos PA, Christensen J, Agger K, Maiolica A, Rappsilber J, Antal T, Hansen KH, Helin K. The putative oncogene GASC1 demethylates tri- and dimethylated lysine 9 on histone H3. Nature. 2006; 442:307–311. [PubMed: 16732293]

Collado M, Gil J, Efeyan A, Guerra C, Schuhmacher AJ, Barradas M, Benguria A, Zaballos A, Flores JM, Barbacid M, et al. Tumour biology: senescence in premalignant tumours. Nature. 2005; 436:642. [PubMed: 16079833]

Coppe JP, Desprez PY, Krtolica A, Campisi J. The senescence-associated secretory phenotype: the dark side of tumor suppression. Annu Rev Pathol. 2010; 5:99–118. [PubMed: 20078217]

Coppé JP, Patil CK, Rodier F, Sun Y, Munoz DP, Goldstein J, Nelson PS, Desprez PY, Campisi J. Senescence-associated secretory phenotypes reveal cell-nonautonomous functions of oncogenic RAS and the p53 tumor suppressor. PLoS Biol. 2008; 6:2853–2868. [PubMed: 19053174]

Dankort D, Curley DP, Cartlidge RA, Nelson B, Karnezis AN, Damsky WE Jr, You MJ, DePinho RA, McMahon M, Bosenberg M. Braf(V600E) cooperates with Pten loss to induce metastatic melanoma. Nat Genet. 2009; 41:544–552. [PubMed: 19282848]

Dhomen N, Reis-Filho JS, da Rocha Dias S, Hayward R, Savage K, Delmas V, Larue L, Pritchard C, Marais R. Oncogenic Braf induces melanocyte senescence and melanoma in mice. Cancer Cell. 2009; 15:294–303. [PubMed: 19345328]

Di Micco R, Fumagalli M, Cicalese A, Piccinin S, Gasparini P, Luise C, Schurra C, Garre' M, Nuciforo PG, Bensimon A, et al. Oncogene-induced senescence is a DNA damage response triggered by DNA hyper-replication. Nature. 2006; 444:638–642. [PubMed: 17136094]

Dimri GP, Lee X, Basile G, Acosta M, Scott G, Roskelley C, Medrano EE, Linskens M, Rubelj I, Pereira-Smith O, et al. A biomarker that identifies senescent human cells in culture and in aging skin in vivo. Proc Natl Acad Sci USA. 1995; 92:9363–9367. [PubMed: 7568133]

Dobin A, Davis CA, Schlesinger F, Drenkow J, Zaleski C, Jha S, Batut P, Chaisson M, Gingeras TR. STAR: ultrafast universal RNA-seq aligner. Bioinformatics. 2013; 29:15–21. [PubMed: 23104886]

Dorr JR, Yu Y, Milanovic M, Beuster G, Zasada C, Dabritz JH, Lisec J, Lenze D, Gerhardt A, Schleicher K, et al. Synthetic lethal metabolic targeting of cellular senescence in cancer therapy. Nature. 2013; 501:421–425. [PubMed: 23945590]

Ederveen TH, Mandemaker IK, Logie C. The human histone H3 complement anno 2011. Biochim Biophys Acta. 2011; 1809:577–586. [PubMed: 21782046]

Euhus DM, Hudd C, LaRegina MC, Johnson FE. Tumor measurement in the nude mouse. J Surg Oncol. 1986; 31:229–234. [PubMed: 3724177]

Gartner JJ, Parker SC, Prickett TD, Dutton-Regester K, Stitzel ML, Lin JC, Davis S, Simhadri VL, Jha S, Katagiri N, et al. Whole-genome sequencing identifies a recurrent functional synonymous mutation in melanoma. Proc Natl Acad Sci USA. 2013; 110:13481–13486. [PubMed: 23901115]

Haferkamp S, Borst A, Adam C, Becker TM, Motschenbacher S, Windhovel S, Hufnagel AL, Houben R, Meierjohann S. Vemurafenib induces senescence features in melanoma cells. J Invest Dermatol. 2013; 133:1601–1609. [PubMed: 23321925]

Hanahan D, Weinberg RA. Hallmarks of cancer: the next generation. Cell. 2011; 144:646–674. [PubMed: 21376230]

Haupt Y, Harris AW, Adams JM. Retroviral infection accelerates T lymphomagenesis in Eμ-N-ras transgenic mice by activating c-myc or N-myc. Oncogene. 1992; 7:981–986. [PubMed: 1570158]

Huang J, Sengupta R, Espejo AB, Lee MG, Dorsey JA, Richter M, Opravil S, Shiekhattar R, Bedford MT, Jenuwein T, et al. p53 is regulated by the lysine demethylase LSD1. Nature. 2007; 449:105–108. [PubMed: 17805299]

Ishimura A, Terashima M, Kimura H, Akagi K, Suzuki Y, Sugano S, Suzuki T. Jmjd2c histone demethylase enhances the expression of Mdm2 oncogene. Biochem Biophys Res Commun. 2009; 389:366–371. [PubMed: 19732750]

Jacks T, Remington L, Williams BO, Schmitt EM, Halachmi S, Bronson RT, Weinberg RA. Tumor spectrum analysis in p53-mutant mice. Curr Biol. 1994; 4:1–7. [PubMed: 7922305]

Jing H, Kase J, Dorr JR, Milanovic M, Lenze D, Grau M, Beuster G, Ji S, Reimann M, Lenz P, et al. Opposing roles of NF-kB in anti-cancer treatment outcome unveiled by cross-species investigations. Genes Dev. 2011; 25:2137–2146. [PubMed: 21979374]

Johnson L, Mercer K, Greenbaum D, Bronson RT, Crowley D, Tuveson DA, Jacks T. Somatic activation of the K-ras oncogene causes early onset lung cancer in mice. Nature. 2001; 410:1111–1116. [PubMed: 11323676]

Kang TW, Yevsa T, Woller N, Hoenicke L, Wuestefeld T, Dauch D, Hohmeyer A, Gereke M, Rudalska R, Potapova A, et al. Senescence surveillance of pre-malignant hepatocytes limits liver cancer development. Nature. 2011; 479:547–551. [PubMed: 22080947]

Kemper K, Krijgsman O, Kong X, Cornelissen-Steijger P, Shahrabi A, Weeber F, van der Velden DL, Bleijerveld OB, Kuilman T, Kluin RJ, et al. BRAF(V600E) kinase domain duplication identified in therapy-refractory melanoma patient-derived xenografts. Cell Rep. 2016; 16:263–277. [PubMed: 27320919]

King ON, Li XS, Sakurai M, Kawamura A, Rose NR, Ng SS, Quinn AM, Rai G, Mott BT, Beswick P, et al. Quantitative high-throughput screening identifies 8-hydroxyquinolines as cell-active histone demethylase inhibitors. PLoS One. 2010; 5:e15535. [PubMed: 21124847]

Kopylova E, Noé L, Touzet H. SortMeRNA: fast and accurate filtering of ribosomal RNAs in metatranscriptomic data. Bioinformatics. 2012; 28:3211–3217. [PubMed: 23071270]

Kuilman T, Michaloglou C, Vredeveld LC, Douma S, van Doorn R, Desmet CJ, Aarden LA, Mooi WJ, Peeper DS. Oncogene-induced senescence relayed by an interleukin-dependent inflammatory network. Cell. 2008; 133:1019–1031. [PubMed: 18555778]

Kuilman T, Peeper DS. Senescence-messaging secretome: SMS-ing cellular stress. Nat Rev Cancer. 2009; 9:81–94. [PubMed: 19132009]

Littlewood TD, Hancock DC, Danielian PS, Parker MG, Evan GI. A modified oestrogen receptor ligand-binding domain as an improved switch for the regulation of heterologous proteins. Nucleic Acids Res. 1995; 23:1686–1690. [PubMed: 7784172]

Mallette FA, Richard S. JMJD2A promotes cellular transformation by blocking cellular senescence through transcriptional repression of the tumor suppressor CHD5. Cell Rep. 2012; 2:1233–1243. [PubMed: 23168260]

Mann MB, Black MA, Jones DJ, Ward JM, Yew CC, Newberg JY, Dupuy AJ, Rust AG, Bosenberg MW, McMahon M, et al. Transposon mutagenesis identifies genetic drivers of Braf(V600E) melanoma. Nat Genet. 2015; 47:486–495. [PubMed: 25848750]

Maze I, Wenderski W, Noh KM, Bagot RC, Tzavaras N, Purushothaman I, Elsasser SJ, Guo Y, Ionete C, Hurd YL, et al. Critical role of histone turnover in neuronal transcription and plasticity. Neuron. 2015; 87:77–94. [PubMed: 26139371]

Metzger E, Wissmann M, Yin N, Muller JM, Schneider R, Peters AH, Gunther T, Buettner R, Schule R. LSD1 demethylates repressive histone marks to promote androgen-receptor-dependent transcription. Nature. 2005; 437:436–439. [PubMed: 16079795]

Michaloglou C, Vredeveld LC, Soengas MS, Denoyelle C, Kuilman T, van der Horst CM, Majoor DM, Shay JW, Mooi WJ, Peeper DS. BRAFE600-associated senescence-like cell cycle arrest of human naevi. Nature. 2005; 436:720–724. [PubMed: 16079850]

Milanovic M, Fan DNY, Belenki D, Däbritz JHM, Zhao Z, Yu Y, Dörr JR, Dimitrova L, Lenze D, Monteiro Barbosa IA, et al. Senescence-associated reprogramming promotes cancer stemness. Nature. 2018; 553:96–100. [PubMed: 29258294]

Mooi WJ, Peeper DS. Oncogene-induced cell senescence–halting on the road to cancer. N Engl J Med. 2006; 355:1037–1046. [PubMed: 16957149]

Narita M, Nunez S, Heard E, Lin AW, Hearn SA, Spector DL, Hannon GJ, Lowe SW. Rb-mediated heterochromatin formation and silencing of E2F target genes during cellular senescence. Cell. 2003; 113:703–716. [PubMed: 12809602]

Nicholson TB, Chen T. LSD1 demethylates histone and non-histone proteins. Epigenetics. 2009; 4:129–132. [PubMed: 19395867]

Nielsen SJ, Schneider R, Bauer UM, Bannister AJ, Morrison A, O'Carroll D, Firestein R, Cleary M, Jenuwein T, Herrera RE, et al. Rb targets histone H3 methylation and HP1 to promoters. Nature. 2001; 412:561–565. [PubMed: 11484059]

Patton EE, Widlund HR, Kutok JL, Kopani KR, Amatruda JF, Murphey RD, Berghmans S, Mayhall EA, Traver D, Fletcher CD, et al. BRAF mutations are sufficient to promote nevi formation and cooperate with p53 in the genesis of melanoma. Curr Biol. 2005; 15:249–254. [PubMed: 15694309]

Peeper DS, Dannenberg JH, Douma S, te Riele H, Bernards R. Escape from premature senescence is not sufficient for oncogenic transformation by Ras. Nat Cell Biol. 2001; 3:198–203. [PubMed: 11175753]

Peters AH, O'Carroll D, Scherthan H, Mechtler K, Sauer S, Schofer C, Weipoltshammer K, Pagani M, Lachner M, Kohlmaier A, et al. Loss of the Suv39h histone methyltransferases impairs mammalian heterochromatin and genome stability. Cell. 2001; 107:323–337. [PubMed: 11701123]

Piao L, Suzuki T, Dohmae N, Nakamura Y, Hamamoto R. SUV39H2 methylates and stabilizes LSD1 by inhibiting polyubiquitination in human cancer cells. Oncotarget. 2015; 6:16939–16950. [PubMed: 26183527]

Pollock JA, Larrea MD, Jasper JS, McDonnell DP, McCafferty DG. Lysine-specific histone demethylase 1 inhibitors control breast cancer proliferation in ERalpha-dependent and -independent manners. ACS Chem Biol. 2012; 7:1221–1231. [PubMed: 22533360]

Postow MA, Chesney J, Pavlick AC, Robert C, Grossmann K, McDermott D, Linette GP, Meyer N, Giguere JK, Agarwala SS, et al. Nivolumab and ipilimumab versus ipilimumab in untreated melanoma. N Engl J Med. 2015; 372:2006–2017. [PubMed: 25891304]

Pribluda A, Elyada E, Wiener Z, Hamza H, Goldstein RE, Biton M, Burstain I, Morgenstern Y, Brachya G, Billauer H, et al. A senescence-inflammatory switch from cancer-inhibitory to cancer-promoting mechanism. Cancer Cell. 2013; 24:242–256. [PubMed: 23890787]

Rea S, Eisenhaber F, O'Carroll D, Strahl BD, Sun ZW, Schmid M, Opravil S, Mechtler K, Ponting CP, Allis CD, et al. Regulation of chromatin structure by site-specific histone H3 methyltransferases. Nature. 2000; 406:593–599. [PubMed: 10949293]

Reimann M, Lee S, Loddenkemper C, Dörr JR, Tabor V, Aichele P, Stein H, Dörken B, Jenuwein T, Schmitt CA. Tumor stroma-derived TGF-β limits Myc-driven lymphomagenesis via Suv39h1-dependent senescence. Cancer Cell. 2010; 17:262–272. [PubMed: 20227040]

Robert C, Karaszewska B, Schachter J, Rutkowski P, Mackiewicz A, Stroiakovski D, Lichinitser M, Dummer R, Grange F, Mortier L, et al. Improved overall survival in melanoma with combined dabrafenib and trametinib. N Engl J Med. 2015; 372:30–39. [PubMed: 25399551]

Schmitt CA. Senescence, apoptosis and therapy—cutting the lifelines of cancer. Nat Rev Cancer. 2003; 3:286–295. [PubMed: 12671667]

Schmitt CA, McCurrach ME, de Stanchina E, Wallace-Brodeur RR, Lowe SW. INK4a/ARF mutations accelerate lymphomagenesis and promote chemoresistance by disabling p53. Genes Dev. 1999; 13:2670–2677. [PubMed: 10541553]

Schmitt CA, Yang M, Fridman JS, Baranov E, Hoffman RM, Lowe SW. Dissecting p53 tumor suppressor functions in vivo. Cancer Cell. 2002; 1:289–298. [PubMed: 12086865]

Serrano M, Lin AW, McCurrach ME, Beach D, Lowe SW. Oncogenic ras provokes premature cell senescence associated with accumulation of p53 and p16INK4a. Cell. 1997; 88:593–602. [PubMed: 9054499]

Shi Y, Lan F, Matson C, Mulligan P, Whetstine JR, Cole PA, Casero RA. Histone demethylation mediated by the nuclear amine oxidase homolog LSD1. Cell. 2004; 119:941–953. [PubMed: 15620353]

Tamaru H, Selker EU. A histone H3 methyltransferase controls DNA methylation in *Neurospora crassa*. Nature. 2001; 414:277–283. [PubMed: 11713521]

Todaro GJ, Green H. Quantitative studies of the growth of mouse embryo cells in culture and their development into established lines. J Cell Biol. 1963; 17:299–313. [PubMed: 13985244]

VanBrocklin MW, Robinson JP, Lastwika KJ, Khoury JD, Holmen SL. Targeted delivery of NRASQ61R and Cre-recombinase to post-natal melanocytes induces melanoma in Ink4a/Arflox/lox mice. Pigment Cell Melanoma Res. 2010; 23:531–541. [PubMed: 20444198]

Vredeveld LC, Possik PA, Smit MA, Meissl K, Michaloglou C, Horlings HM, Ajouaou A, Kortman PC, Dankort D, McMahon M, et al. Abrogation of BRAFV600E-induced senescence by PI3K pathway activation contributes to melanomagenesis. Genes Dev. 2012; 26:1055–1069. [PubMed: 22549727]

Whetstine JR, Nottke A, Lan F, Huarte M, Smolikov S, Chen Z, Spooner E, Li E, Zhang G, Colaiacovo M, et al. Reversal of histone lysine trimethylation by the JMJD2 family of histone demethylases. Cell. 2006; 125:467–481. [PubMed: 16603238]

Wissmann M, Yin N, Muller JM, Greschik H, Fodor BD, Jenuwein T, Vogler C, Schneider R, Gunther T, Buettner R, et al. Cooperative demethylation by JMJD2C and LSD1 promotes androgen receptor-dependent gene expression. Nat Cell Biol. 2007; 9:347–353. [PubMed: 17277772]

Xue W, Zender L, Miething C, Dickins RA, Hernando E, Krizhanovsky V, Cordon-Cardo C, Lowe SW. Senescence and tumour clearance is triggered by p53 restoration in murine liver carcinomas. Nature. 2007; 445:656–660. [PubMed: 17251933]

Zhang R, Poustovoitov MV, Ye X, Santos HA, Chen W, Daganzo SM, Erzberger JP, Serebriiskii IG, Canutescu AA, Dunbrack RL, et al. Formation of MacroH2A-containing senescence-associated heterochromatin foci and senescence driven by ASF1a and HIRA. Dev Cell. 2005; 8:19–30. [PubMed: 15621527]

Highlights

- H3K9me3-active demethylases like LSD1 or JMJD2C disable oncogene-induced senescence
- LSD1 or JMJD2C cooperate with activated Braf in animal models of melanomagenesis
- Human melanoma samples co-overexpress structurally unrelated H3K9 demethylases
- H3K9 demethylase targeting blocks melanoma growth by restoring senescence

Significance

Structurally unrelated flavin-dependent (e.g., LSD1) and 2-oxoglutarate-dependent (e.g., JMJD2C) demethylases are frequently found to be overexpressed in various cancer entities, but their oncogenic mode of action remains unclear. We present here the overlapping and cooperative oncogenic activity of distinct H3K9me3-active demethylases at the nevus-to-melanoma transition in Ras/Braf-driven model systems and primary patient samples, thereby underscoring the essential, albeit dynamic, role of the H3K9me3 mark in oncogene-induced senescence, and uncovering H3K9 demethylase net activity as melanoma vulnerability. Our study provides a mechanistic basis for H3K9 demethylase targeting in cancer with critical implications for targeted and immune-based treatment strategies.

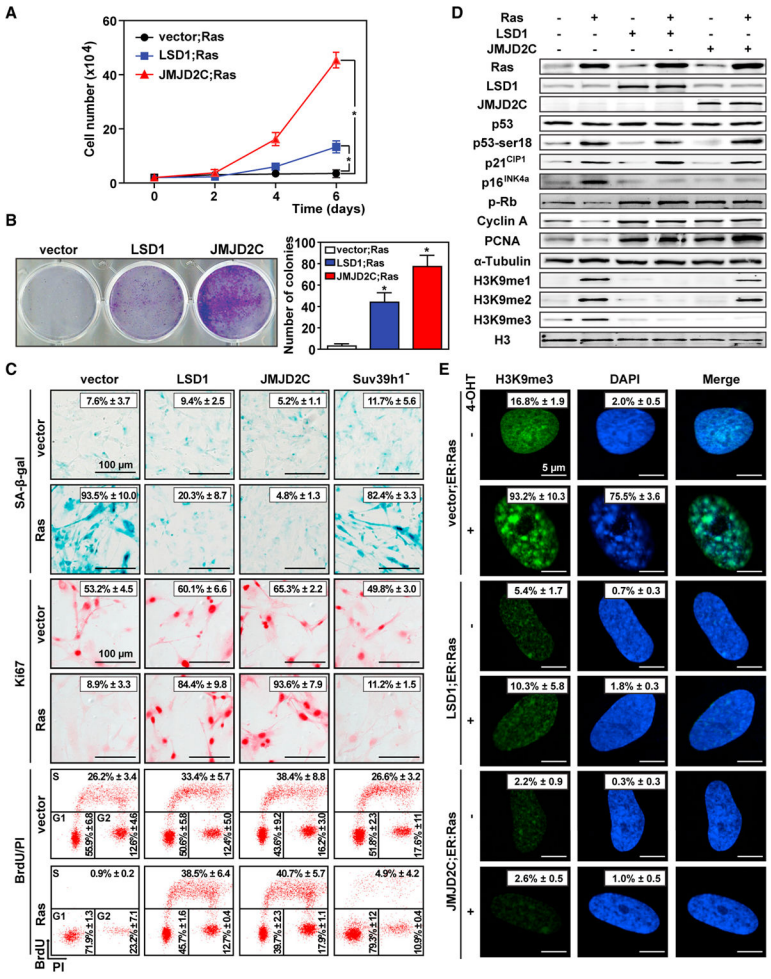

Figure 1. H3K9me3-Active Histone Demethylases Inhibit Ras-Induced Senescence

(A) Growth of Ras-expressing MEFs stably expressing LSD1, JMJD2C, or an empty vector as a control.

(B) Colony-formation assay of MEFs as in (A); representative photos of crystal violet-stained wells (left), and quantification (right).

(C) SA-β-gal staining, immunocytochemical detection of Ki67, and BrdU/PI-based cell-cycle analysis of MEFs as in (A). Note that Suv39h1-deficient MEFs still senesce (Narita et al., 2003).

(D) Immunoblot analyses of the indicated proteins in cell lysates from MEFs as in (C) with α-tubulin or total H3 as loading controls.

(E) Representative photos of H3K9me3 detection by immunofluorescence in Tig3 HDFs stably expressing a 4-OHT-inducible estrogen receptor (ER) to oncogenic Ras fusion (ER:Ras); DAPI staining marks nuclei.

All data reflect at least three independent experiments, and are presented as mean values ± SD. *p < 0.05. See also Figure S1.

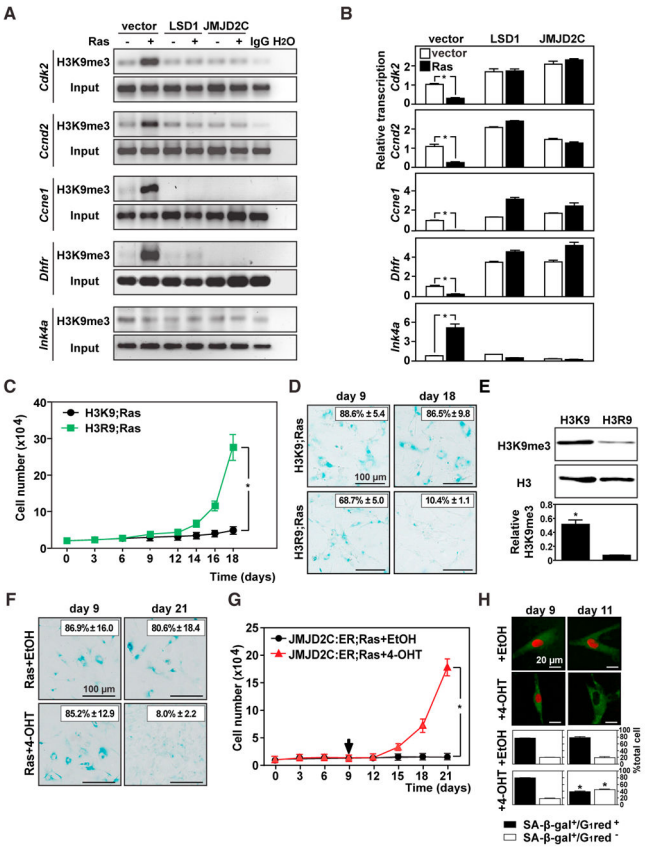

Figure 2. The H3K9me3 Mark Operates as an Essential Senescence Relay

(A) ChIP assays of MEFs as presented in Figure 1, using an H3K9me3 antibody and PCR primers specific for promoters of E2F target genes (*Cdk2*, *Ccnd2*, *Ccne1*, *Dhfr*) and *Ink4a* as a non-E2F target gene control. Input (no immunoprecipitation) as internal control. Anti-immunoglobulin G (IgG) as a non-specific antibody and H_2O (no input) were used as negative controls.

(B) qRT-PCR analyses of the indicated transcripts (relative to *Gapdh* as a control).

(C) Growth of Ras-expressing MEFs stably expressing H3R9 or wild-type H3 (H3K9).

(D) SA-β-gal staining at the indicated time points of MEFs as in (C).

(E) Immunoblot analyses of H3K9me3, total H3 as a loading control, in lysates from cells as in (D) at day 18. The histogram shows the H3K9me3/total H3 ratio of the scanned bands.

(F and G) SA-β-gal staining at the indicated time points (F) and growth (G) of Ras-senescent MEFs expressing JMJD2C:ER. 4-OHT or ethanol (EtOH) as a solvent control was added on day 9 (arrow).

(H) Cell-cycle/senescence tracking of cells as in (G) over the indicated time points after adding 4-OHT or EtOH. Cells were transduced with a G_1-phase reporter construct (red), and co-stained with the fluorescent substrate C12FDG (green) for SA-β-gal reactivity. The histogram shows the percentage of SA-β-gal-positive cells in or out of G_1 within the entire population (with SA-β-gal$^+$/G_1red$^-$ marking previously senescent cells that just exited the G_1 phase).

All data (except those in A) reflect three independent experiments, and are presented as mean ± SD. *$p < 0.05$. See also Figures S2 and S3.

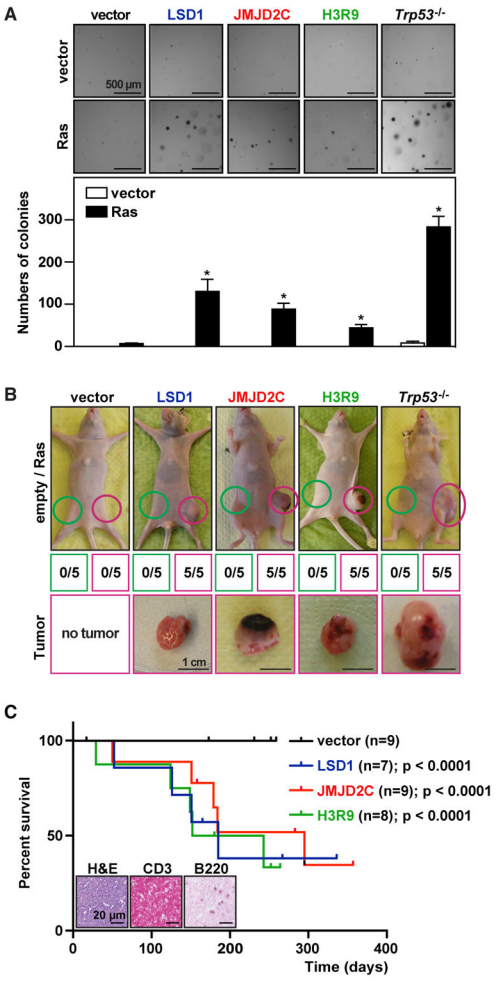

Figure 3. Oncogenic Ras Cooperates with Compromised H3K9 Tri-methylation to Directly Transform Primary MEFs, and to Drive T Cell Lymphomagenesis *In Vivo*

(A) Anchorage-independent colony formation in soft agar of stably Ras-(versus vector)-expressing MEFs co-infected with retroviruses encoding LSD1, JMJD2C, H3R9, or an empty vector. *Trp53*$^{-/-}$ MEFs as a readily Ras-transformable positive control. Representative photos of the colonies formed after 2 weeks (top), and their quantification (bottom; n = 4 independent experiments). Histogram bars indicate mean numbers ± SD. *p < 0.05.

(B) Tumor formation in nude mice. Representative photos of mice (top) at day 20 (JMJD2C and *Trp53*$^{-/-}$) or day 35 (LSD1, H3R9, and vector); note that each group of mice (n = 5) was transplanted with MEFs as indicated, stably expressing Ras in the right (purple circle) or an empty vector in the left flank (green circle). Representative photos of isolated tumors *ex vivo* (bottom); fractions (middle) indicate the tumor incidences.

(C) Kaplan-Meier survival plot of mice transplanted with Eμ-N-Ras transgenic FLC stably expressing LSD1 (red), JMJD2C (blue), H3R9 (green), and an empty vector (black). Insets show representative lymphoma sections stained with the T cell marker CD3 and the B cell marker B220. See also Figure S4.

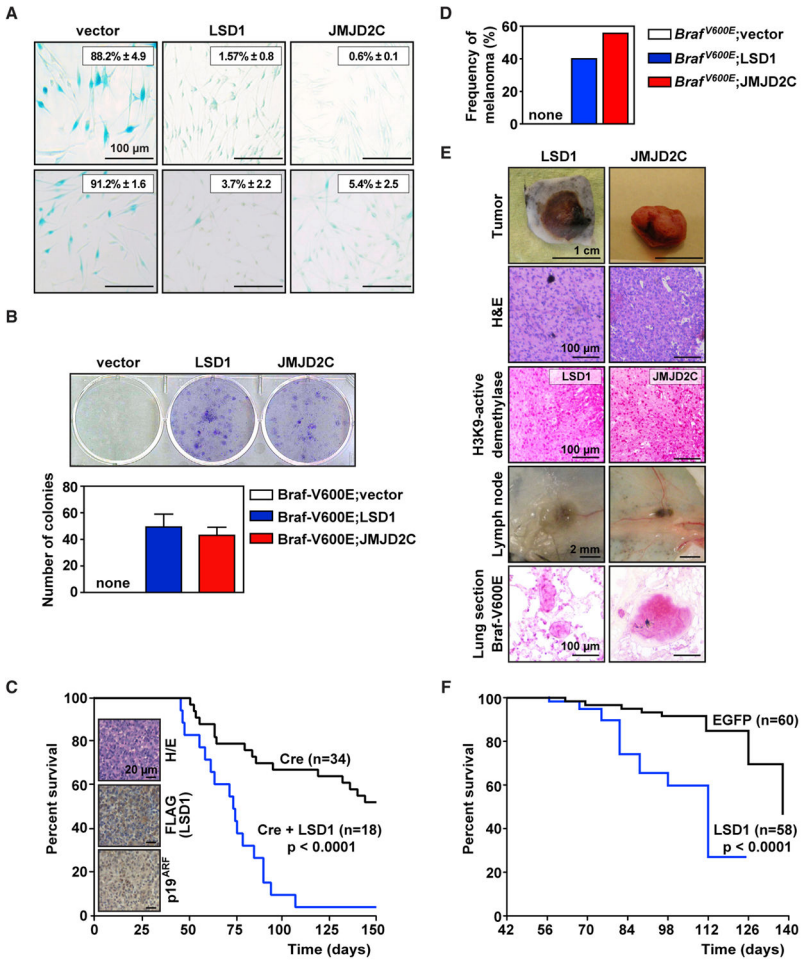

Figure 4. H3K9 Demethylases Overcome Braf-Driven Melanocyte Senescence and Promote Melanomagenesis

(A) SA-β-gal staining of human primary melanocytes, either stably expressing LSD1 or JMJD2C (or a vector control) first, followed by Braf-V600E expression (top), or after expression of these moieties in already Braf-senescent melanocytes (bottom). Numbers indicate mean ± SD.

(B) Colony-formation assay matching the setting in bottom panels of (A). Number of colonies and representative photos of colonies are shown. Data are presented as mean ± SD.

(C) Kaplan-Meier survival plot of *Dct::TVA; Braf*^{CA};*Cdkn2a*$^{lox/lox}$ mice injected with RCAS-Cre virus alone (black) or RCAS-Cre/RCAS-LSD1 virus (blue). Representative photos of tumor sections from LSD1 virus-infected mice stained with H&E and FLAG indicating LSD1 expression and p19^{ARF} expression.

(D) Melanoma development in 4-OHT-pretreated, nevus-carrying *Tyr-Cre:ER*^{T2};*lsl-Braf*^{V600E} mice within 150 days after intralesional injection with LSD1-encoding (n = 5) or JMJD2C-encoding (n = 9) lentivirus.

(E) Representative photos of manifest melanomas *ex vivo*, and tumor sections stained with H&E and antibodies recognizing LSD1 or JMJD2C. Lymph node enlargement and Braf-V600E staining of lung sections marked melanoma metastasis.

(F) Kaplan-Meier plot showing tumor-free survival of Tg(*mitfa:BRAF*^{V600E});*tp53*$^{-/-}$;*mitfa*$^{-/-}$ zebrafish injected with MCR:LSD1 (blue) or MCR:EGFP as control (black).

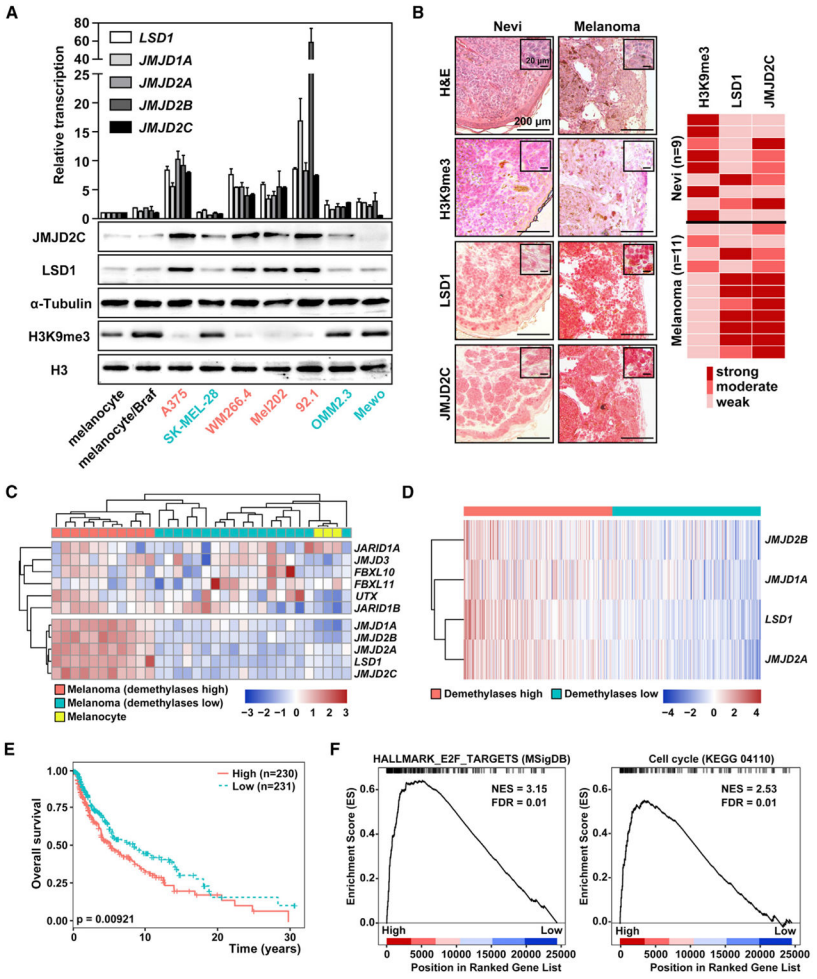

Figure 5. A Distinct Subgroup of Manifest Melanomas Exhibits High-Level Expression across the Class of H3K9-Active Demethylases

(A) Relative expression levels of *LSD1*, *JMJD1A*, *JMJD2A*, *JMJD2B*, and *JMJD2C* transcripts by qRT-PCR (top) and immunoblot analysis of LSD1, JMJD2C, and H3K9me3 (bottom) in primary human melanocytes, Braf-senescent melanocytes, and the indicated human melanoma cell lines. mRNA expression is normalized to the expression in primary melanocytes (conducted in triplicates; histogram bars indicate mean values ± SD). Melanoma cell lines with relative mRNA expression levels of the indicated demethylases consistently <5-fold are marked in green and >5-fold in pink. α-Tubulin and total H3 are loading controls in the immunoblot analysis.

(B) Representative images of H&E and immunohistochemical analysis of the indicated proteins (left) and immunohistochemical staining intensities (right) in individual patient nevi or melanoma biopsies (insets show higher magnification).

(C) Microarray-based gene expression analysis of 29 melanoma patient samples, and normal melanocytes for comparison.

(D) RNA-seq-based gene expression analysis of the TCGA-SKCM dataset, comprising 468 patients with primary or metastatic melanoma. Samples were ordered by average demethylase expression and separated into two groups with above and below average

expression levels. *JMJD2C* was omitted from this analysis as it was only expressed at low levels with little variation across samples.

(E) Kaplan-Meier overall survival analysis comparing patients with high versus low average demethylase expression.

(F) Gene set enrichment analysis profiles of E2F targets and cell-cycle genes between demethylase-high versus -low melanomas. Red colors denote a positive signal-to-noise ratio (SNR) between the two groups, and blue colors indicate a negative SNR. NES, normalized enrichment score; FDR, false discovery rate (Benjamini and Hochberg) adjusted p value. See also Figure S5.

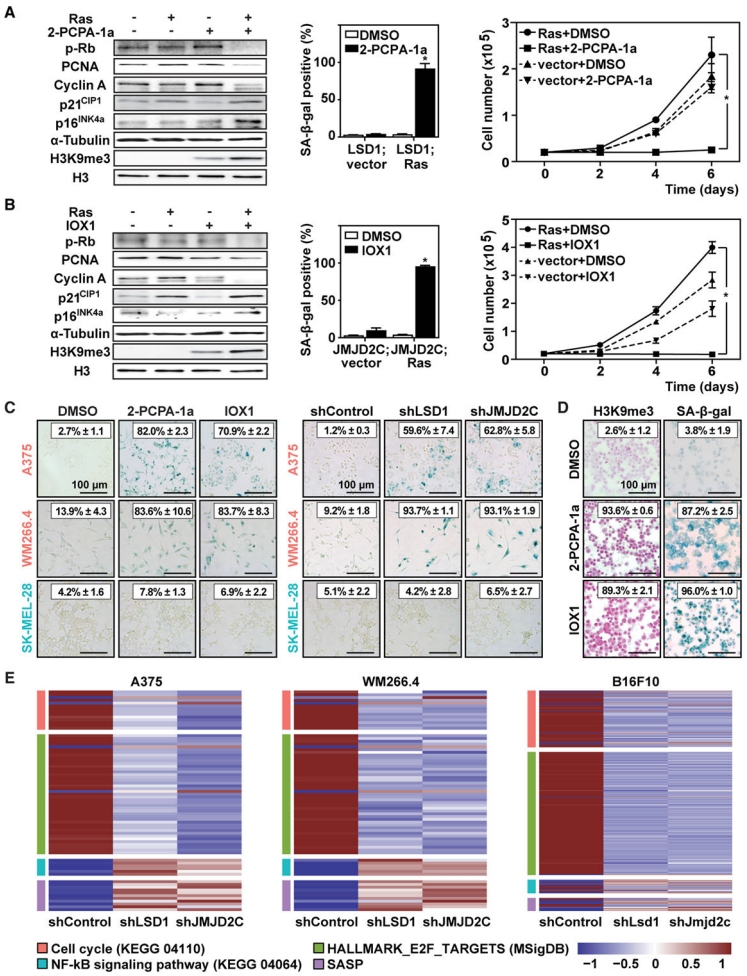

Figure 6. Specific Demethylase Inhibition Restores OIS in LSD1- or JMJD2C-Overexpressing Fibroblasts and Melanoma Cell Lines

(A and B) Characterization of MEFs stably expressing oncogenic Ras or a vector control overexpressing LSD1 treated with 2-PCPA-1a (A) or overexpressing JMJD2C treated with IOX1 (B), DMSO as a solvent control in both, assessed by immunoblot analysis of the indicated proteins (left), percentage of SA-β-gal reactivity (middle), and growth curve analysis (right).

(C) SA-β-gal staining of human melanoma cell lines (A375 and WM266.4 representing the demethylase-high group [pink], and SK-MEL-28 representing the demethylase-low group [green]) 5 days after exposure to the indicated inhibitors (left) or knockdown of gene expression (right; scrambled shRNA as a control).

(D) Patient-derived DMC exposed to 2-PCPA-1a, IOX1, or DMSO as a solvent control for 7 days, stained for H3K9me3 and SA-β-gal activity.

(E) RNA-seq analyses of melanoma cell lines A375, WM266.4, and B16F10 after senescence restoration by knockdown of indicated demethylases. Shown are the expression patterns of differentially expressed genes (adjusted $p < 0.05$), in senescence-relevant gene sets.

All experiments (except those in E) were conducted in triplicate, and numbers indicate mean values or mean percentages of positive cells ± SD. *$p < 0.05$. See also Figure S6.

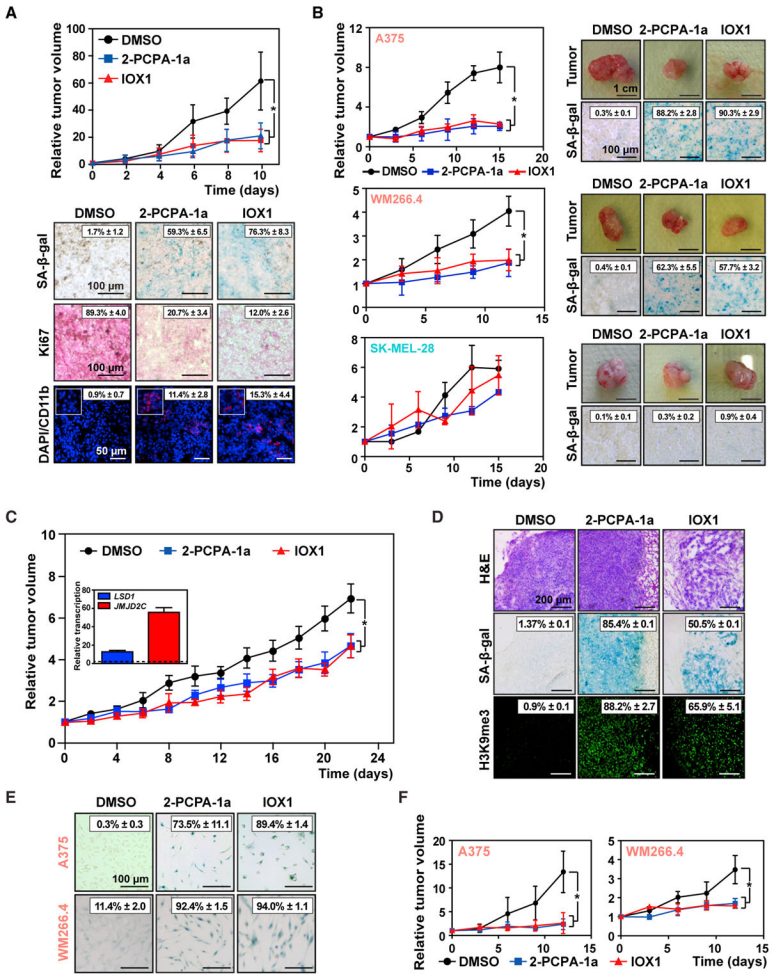

Figure 7. Melanoma-Bearing Mice Are Susceptible to Senescence-Restoring LSD1 or JMJD2C Inhibitor Treatment

(A) Growth (top) and representative tumor sections at the end of treatment stained for SA-β-gal, Ki67, and CD11b (bottom) of murine B16F10 melanoma cells implanted in syngeneic wild-type mice, and treated with 2-PCPA-1a, IOX1, or DMSO.

(B) Growth curves (left) and representative photos of isolated tumors and corresponding SA-β-gal staining of tumor sections (right) of xenografted human melanoma cell lines in NSG mice subjected to the indicated treatments.

(C) Growth curves of melanoma PDX samples (M032.X2) in mice subjected to the indicated treatments and relative transcript levels of *LSD1* and *JMJD2C* (inset).

(D) Representative photos of tumor sections in (C) at the end of treatment, stained for H&E, SA-β-gal, and H3K9me3.

(E and F) SA-β-gal staining *in vitro* (E) and xenograft growth curve analyses *in vivo* (F) of vemurafenib-resistant derivatives of A375 and WM266.4 melanoma cells with 2-PCPA-1a or IOX1 treatment.

All data are presented as mean ± SD. *p < 0.05. See also Figure S7.